Imidazole-functionalized nitrogen-rich Mg-Al-CO3 layered double hydroxide for developing highly crosslinkable epoxy with high thermal and mechanical properties

Farzad Seidi, Maryam Jouyandeh, Seyed Mohammad Reza Paran, Amin Esmaeili, Zohre Karami, Sébastien Livi, Sajjad Habibzadeh, Henri Vahabi, Mohammad Reza Ganjali, Mohammad Reza Saeb

Imidazole-functionalized nitrogen-rich Mg-Al-CO_3 layered double hydroxide for developing highly crosslinkable epoxy with high thermal and mechanical properties

Farzad Seidi[a], Maryam Jouyandeh[b,c,*], Seyed Mohammad Reza Paran[b], Amin Esmaeili[d], Zohre Karami[b], Sébastien Livi[e], Sajjad Habibzadeh[f], Henri Vahabi[c,*], Mohammad Reza Ganjali[b,g], Mohammad Reza Saeb[c]

[a] Provincial Key Lab of Pulp and Paper Science and Technology and Joint International Research Lab of Lignocellulosic Functional Materials, Nanjing Forestry University, Nanjing 210037, China

[b]Center of Excellence in Electrochemistry, School of Chemistry, College of Science, University of Tehran, Iran

[c]Université de Lorraine, CentraleSupélec, LMOPS, F-57000 Metz, France

[d]Department of Chemical Engineering, School of Engineering Technology and Industrial Trades, College of the North Atlantic—Qatar, Arab League St, Doha 24449, Qatar

[e]Univ Lyon, INSA Lyon, CNRS, IMP UMR 5223, F-69621, Villeurbanne, France

[f]Department of Chemical Engineering, Amirkabir University of Technology (Tehran Polytechnic), Tehran, Iran

[g]Biosensor Research Center, Endocrinology and Metabolism Molecular-Cellular Sciences Institute, Tehran University of Medical Sciences, Tehran, Iran

To whom correspondence should be addressed:

* Maryam Jouyandeh, PhD.; E-mail: maryam.jouyande@gmail.com

* Henri Vahabi, PhD; E-mail: henri.vahabi@univ-lorraine.fr

Abstract

Ionic liquid-based N-octadecyl-N'-octadecyl imidazolium iodide functionalized layered double hydroxide (LDH-IM) was synthesized for manufacturing high-performance epoxy nanocomposites. Nonisothermal differential scanning calorimetry (DSC) was performed to study cure kinetics of epoxy nanocomposites with LDH and LDH-IM. Incorporation of Mg-Al-CO_3 LDH into epoxy hindered the curing reaction, as detected by dimensionless *Cure Index* (*CI*). By contrast, epoxy/LDH-IM cured *Good* and *Excellent* due to imidazolium ionic liquid. Higher activation energy for completely cured epoxy/LDH-IM nanocomposite was obtained compared to epoxy and epoxy/LDH nanocomposites. The curing reaction rate was obtained by calculation of the orders of instantaneous autocatalytic and non-catalytic reactions, and optimal kinetic parameters based on isoconversional methods were in good agreement with experimental cure reaction rates. Lower value of T_g for epoxy/LDH nanocomposite compared to the neat epoxy signified weak interactions between Mg-Al-CO_3-LDH and epoxy matrix, while a higher T_g was obtained for epoxy/LDH-IM. Network degradation kinetics of the samples was also investigated. The higher decomposition activation energy for epoxy/LDH-IM approved strong interfacial adhesion in the assigned system. The highly reactive nature of the developed LDH-IM gives reason for its usage for developing highly curable epoxy with high thermal and mechanical properties.

Keyword: Layered double hydroxide (LDH); Imidazolium ionic liquids; Epoxy; Cure kinetics; Thermal decomposition kinetics

1. Introduction

Polymer scientists and technologists alike are seeking nanoparticles with appropriate dispersion in polymers for developing high-performance polymer nanocomposites [1-3]. Analyses made on thermal stability, mechanical, anti-corrosive, and flame retardant properties of nanocomposites unraveled difficulties in developing toughened epoxy systems [4-8]. Strategically, the use of reactive liquid rubbers was proposed as a solution to produce toughened epoxy resins [9, 10]. By contrast, network formation in epoxy containing nanoparticles was occasionally addressed [11-13]. Available reports address the effects of the size, shape, and functionality of nanoparticles on the properties of epoxy [14-16]. An additional requirement is to find low-cost nanoparticles. Complexity of finding a nanoparticle that could meet requirements (low cost/easily dispersible/highly reactive) has always been a driving force behind developing advanced polymer composites [17].

The abundance, low cost, low toxicity and special shape of clay minerals were reasons behind the use of clays in developing organic coatings [18, 19]. Typically, cationic clays or clay minerals (available in nature) and anionic clays or layered double hydroxides (LDH) (available in the laboratory or industrial scale) are known as the main general classes of clays [20]. Cationic clays are negatively charged with alumina-silicate layers with small cations in between the interlayer space to balance the charge. By contrast, anionic clays have positive charges in between brucite-like metal hydroxide layers with balancing anions and water molecules in their interlayer space [21]. The exchange and arrangement of guest species in interlayer space and the degree of the order-disorder transformation allow one for developing diverse LDH derivatives for a wide range of applications [22, 23].

The most frequently available molecular structure of LDH is shown by **Eq. (1)** [24]:

$$[M^{2+}_{1-x}M^{3+}_{x}(OH)_2]^{x+} (A^{n-})_{x/n}.yH_2O \quad (1)$$

where M^{2+} is a divalent metal ion such as Mg^{2+}, Ca^{2+} or Zn^{2+} [25, 26], M^{3+} is a trivalent metal ion such as Al^{3+}, Cr^{3+}, Fe^{3+} or Co^{3+} [27], and eventually A^{n-} is an anion such as Cl^-, CO_3^{2-} or NO_3^- [28, 29]. Depending on brucite-like layer of $[M^{2+}_{1-x}M^{3+}_{x}(OH)_2]^{x+}$, basal value *d*, and as a result of using intercalating agents the LDH interlamellar space *l* will be changed to attain a wide variety of LDH structures.

When an intercalating agent is used, the general formula of the modified (sometimes known as intercalated) LDH can be reformed to **Eq. (2)**:

$$[M^{2+}_{1-x}M^{3+}_{x}(OH)_2]^{x+} [(A^{n-})_{x/n}.yH_2O]^{x-} \quad (2)$$

where A^{n-} is the intercalating anion (or anions).

A wide variety of LDH structures have been taken into account in preparation of epoxy composites, in which nanoplatelets were directly mixed with epoxy resin followed by addition of curing agent. *In situ* polymerization of epoxy monomer in the presence of nanoparticles was also examined [30, 31]. Depending on the intercalation degree of clay platelets [32, 33], a wide variety of morphologies have been observed in polymer/LDH nanocomposites, which strongly affected the properties of epoxy [34, 35].

For epoxy/LDH nanocomposites, significant changes in the ultimate properties/performance ranging from thermal and mechanical to flame retardancy were reported upon manipulation of LDH structure as well as the enlargement of interlayer space between layered nanoplatelets [36,

37]. It was reported that addition of LDH with NO_2^- intercalating anion to the lamella structures the barrier performance of epoxy coating was improved [38]. Incorporation of 0.05 mass% of MgAl-NO_3 LDH increased the anticorrosion performance of coating through impedance increase from 4.64×10^8 Ω cm^2 for neat epoxy to 2.14×10^{10} Ω cm^2 for nanocomposite. Elsewhere, sodium phenyl phosphate intercalated CuAl-LDH effectively improved the flame retardancy and smoke suppression performance of epoxy [39]. It was indicated that the peak of heat release rate and the peak of smoke production rate of epoxy containing sodium phenyl phosphate intercalated CuAl-LDH were decreased 55.6% and 46.2%, respectively. Nevertheless, reports on curing potential of epoxy/LDH nanocomposites are limited to glass transition temperature (T_g) or the exothermic peak displacements in nonisothermal differential scanning calorimetry (DSC). For example, it was reported that increasing the molar mass of poly(oxypropylene)–amindocarboxylic intercalating agent was responsible for its higher thermal stability because of enlargement of the interlamellar space [40]. It was also observed that higher contents of modified LDH (10 mass%) decreased significantly the exothermic peak of DSC thermograms from 182 to 152°C.

In a previous work [41], two types of LDH were used and the significant change in cure kinetics was reflected in the reduction of the activation energy by zinc (Zn) compared to magnesium (Mg), due to the action of Zn metal as an adduct with epoxy group. Moreover, sodium dodecylbenzene sulfonate was used to enlarge the interlamellar space, and also to enhance the degree of compatibility of LDH with hydrophobic epoxy matrix. The *Cure Index* (*CI*) and thermomechanical properties of epoxy/Mg-Al-NO_3LDH system were high, like the storage modulus and α-relaxation temperature (T_α). Interpretations based on T_g were indicative of larger

interlayer space of Mg-Al nanoplatelets. Moreover, the role of intercalated anion in epoxide ring opening reaction was also explored by the aid of the *CI* [42-44].

In recent years, using ionic liquids and liquid crystal precursors in epoxy received much more attention. Improvement of thermal conductivity [45, 46], flame retardancy [47] and mechanical properties [48] of epoxy resin by the use of liquid precursors was the subject of several reports [49]. The presence of both organic cation and anion in the ionic liquids structure gives them the possibility to be served for functionalization of both cationic and anionic clay minerals. Modification of cationic clay minerals with diverse ionic liquids has been studied by many researchers [50-53]. Nevertheless, less attention has been paid to modify anionic clay minerals (LDH) with ionic liquids [54-56]. In addition, modification of nanoparticles with highly reactive ionic liquids and the correlation between cure kinetics and properties was not addressed. Herein, we used N-octadecyl-N'-octadecyl imidazolium iodide (IM) ionic liquid as intercalating agent in synthesis of LDH. The product was characterized by X-ray diffraction analysis (XRD), thermogravimetric analysis (TGA) and transmission electron microscopy (TEM). Cure potential of epoxy/Mg-Al-CO_3-LDH-IM nanocomposites was qualitatively assessed by nonisothermal DSC analyses (25-300°C) based on dimensionless *CI* [57]. Cure kinetics parameters and the activation energy of the cure reaction were modeled by *Friedman* and Kissinger–Akahira–Sunose (*KAS*) isoconversional methods. Surface free energy values of epoxy networks reinforced with LDH and LDH-IM were also determined. Viscoelastic behaviors and the values of glass transition temperature (T_g) of the neat epoxy, epoxy/LDH and epoxy/LDH-IM were also studied by temperature-sweep dynamic mechanical analysis (DMA) at frequency of 1 Hz. Thermal degradation kinetics of the neat epoxy and its nanocomposites containing 0.5, 2.0 and 5.0 mass%

of LDH and LDH-IM were also studied by TGA data using *Friedman*, *KAS* and Flynn–Wall–Ozawa (*FWO*) isoconversional methods.

2. Experimental

2.1. Materials

A hydrotalcite (aluminum magnesium hydroxy carbonate, Mg-Al-CO_3) denoted PURAL® MG 63 HT was chosen as pristine anionic clay and was provided by Sasol Performance Chemicals. Triphenylphosphine (95%), imidazole (99.5%), octadecyl iodide (95%), and all the solvents i.e. Tetrahydrofuran (THF), sodium methanoate, methyl alcohol and acetonitrile were supplied from Aldrich and used as received. Epoxy resin Renlam CY219 and curing agent REN HY 5161 were purchased from Huntsman, Germany.

2.2. Synthesis of imidazolium ionic liquids

Synthesis of imidazolium ionic liquids was carried out through a multi-stage procedure [58]: First, a solution of sodium methoxide was prepared from 1 eq of sodium using freshly distilled methyl alcohol (10 mL) in a sealed septum, 100 mL round-bottom, three-necked flask equipped with a condenser, under argon atmosphere and magnetic stirring. Then, imidazole (1 eq) diluted in acetonitrile (10 mL) imidazole was added into the stirred mixture of sodium methoxide at room temperature. After 30 min, a white precipitate was observed. The mixture was subsequently concentrated under reduced pressure for 1 h. The dried white powder was dissolved in acetonitrile, and a solution of octadecyl iodide (1 eq) diluted in acetonitrile (10 mL) was then added under an inert atmosphere of nitrogen at room temperature. The resulting mixture was stirred for 1 h and then heated under reflux at 85°C for about 24 h. This procedure was repeated

twice and the solvent was removed by evaporation under vacuum. Finally, purification was done by crystallization in a mixture (75/25) of ethyl acetate/acetonitrile. The synthesis route is shown in **Fig. 1a**.

2.3. Organic modification

To do so, first the LDH composed of carbonate counter anions was heated during 24 hours at 500°C in order to form calcined LDH [59]. Then, based on the anion exchange capacity (AEC = 3.35 meq/g) of the LDH used, 2 AEC of imidazolium ionic liquids, denoted IM, and LDH were added in 200 mL of a mixture of deionized water and tetrahydrofuran (THF) at volume ratio of 3:1. The mixture was subsequently kept under stirring at 60°C for 24 h, the precipitate obtained was then filtered and washed with THF for five times. The residual solvent was evaporated under vacuum and the functionalized LDH was dried for 18 h at 80°C. Modification of LDH by IM is shown schematically in **Fig. 1b**.

2.4. Preparation of epoxy nanocomposites

For preparing epoxy nanocomposites listed in **Table 1**, epoxy resins with a 0.1, 0.5, 2.0 and 5.0 mass% of nanoparticles were sonicated for 10 min and left for 24 h for removal of trapped air bubble. To make epoxy mixtures cured, the hardener was added to the resulting mixture at appropriate ratios at ambient temperature, the ratio of epoxy prepolymer to hardener was 2:1 by mass, as prescribed by the supplier, and it was thoroughly stirred for 3 min to make a homogeneous mixture.

Table 1. Composition of the prepared nanocomposites.

Sample code	Nanoparticle	Content (mass%)
EP	-	0.0
EP/LDH-0.1	LDH	0.1
EP/LDH-0.5	LDH	0.5
EP/LDH-2	LDH	2.0
EP/LDH-5	LDH	5.0
EP/LDH-IM-0.1	LDH-IM	0.1
EP/LDH-IM-0.5	LDH-IM	0.5
EP/LDH-IM-2	LDH-IM	2.0
EP/LDH-IM-5	LDH-IM	5.0

2.5. Characterization

XRD analysis was carried out using a diffractometer (Rigaku-MiniflexII, Japan) to assess the structure of LDH. The CuKα radiation was operated at voltage of 30 kV and current of 15 mA. The diffractograms were recorded with a step of 0.02°, with acquisition time of 2 s in 2θ values in the range of 5° to 70°.

ATR spectra of the LDH and LDH-IM were collected on a Perkin Elmer Spectrum One FTIR Spectrometer. The IR absorptions were recorded in the range of 4000-400 cm^{-1}.

Transmission electron microscopy (TEM) was performed at the Technical Center of Microstructures (University of Lyon) using a Phillips CM 120 microscope operating at 80 kV to characterize the dispersion of thermoplastic phases in the epoxy networks. 60-nm-thick ultrathin sections of samples were obtained using an ultramicrotome equipped with a diamond knife and were then set on copper grids.

TGA analysis was performed on a Setaram Labsys Evo thermogravimetric analyzer (France) at heating rate of 10ºC/min in the temperature range of 30-900ºC under a nitrogen purge of 50

mL/min. In addition, thermal degradation kinetics of the neat epoxy and its nanocomposites containing 0.5, 2 and 5 mass% of LDH and LDH-IM was investigated in the temperature range of 30–900ºC at different heating rates of 5, 10 and 15ºC/min under nitrogen atmosphere.

The curing behavior of epoxy nanocomposites was analyzed by nonisothermal DSC technique, using a Netzsch 200F3 Maia Differential Scanning Calorimeter (Germany) and a 409 PC Luxx Simultaneous Thermal Analyzer (STA). All DSC analyses were performed under nitrogen purging of 50 mL/min. The non-isothermal of epoxy nanocomposites was conducted as follows:

1) The samples were heated from 25 to 300°C at various heating rates: 5, 10 and 15°C/min.

2) For estimating T_g, all the samples at the heating rates of 5, 10 and 15°C/min firstly were reached to 300°C, then cooled to ambient temperature at a constant cooling rate and heated again to 300°C.

Surface free energy of resulting epoxy networks was determined from the sessile drop method using a Dataphysics goniometer with water and diiodomethane used as probe liquids.

DMA was performed in tension mode in multi frequency state. The samples measured approximately 120 μm, thick by 10 mm wide and length was about 50 mm. Very low strain and displacement was applied on epoxy film samples within the linear viscoelastic region. Therefore, the amplitude of deformation (straining) needs to be adjusted inside the range of 0.01% to 0.5%. The DMA experiment was conducted for samples in the temperature range of 20 to 200°C at a heating rate of 3°C/min and frequency of 1 Hz.

3. Results and discussion

3.1. Characterization of the synthesized LDH

Fig. 2 (a) presents the XRD spectra of the LDH and ionic liquid-modified-LDH. The surface treatment of LDH by the imidazolium ionic liquid denoted Im-C18 had no influence on the intercalation of ionic liquid with LDH layers. In both cases, one reflection at $2\theta = 11.5°$ was observed corresponding to the basal value (7.7 Å) of the LDH. Therefore, the XRD result showed no contribution from the intercalation between the ionic liquid and clay layers to structural changes, so that the corresponding basal spacing of the LDH was remained almost unaffected. This observation elucidates that the interlayer anion does not change during the modification because of the horizontal orientation of carbonate ions in the gallery space of LDH. As a result, a strong interaction between the carbonate ions and hydroxide layers and also with imidazolium cation remains physisorbed on the LDH surface during modification [60, 61]. However, these results can be explained by the size of the counter anion leading to a planar configuration such as monolayer type. The anions have only one carbonyl bond (C=O) and if theses anions assume a planar configuration, no difference can be observed by XRD.

The FTIR spectra of LDH and imidazolium-based ionic liquid modified LDHs are presented in **Fig. 2**. According to **Fig. 2 (b)**, an adsorption bond at ca. 3450 cm^{-1} can be attributed to the asymmetrical and symmetrical stretching mode of -OH bonds of interlayer water and hydroxide layers [62]. Moreover, a sharp adsorption peak at 1360 cm^{-1} can be assigned to the stretching vibration of carbonate anions located into the interlayer of both the LDH and modified LDH [63]. The FTIR spectrum of LDH-IM shows the C-H in-plane-bending at 1180 cm^{-1}, which is ascribed to the imidazole molecules [64]. Moreover, vibration bands at 757, 651 and 549 cm^{-1}

demonstrate the C-H out-of-plane-bending and ring deformation out-of-plane bending of imidazolium-based ionic liquid in modified LDH structure [64].

After the surface treatment of the LDH by the imidazolium ionic liquids, the thermal degradation of the LDH-IM was investigated by TGA analysis and was represented in **Fig. 2 (c)**. Typically, LDH undergoes three decomposition stages including the loss of water molecules physically trapped in between LDH layers (50-250°C) [56, 65, 66], the removal of interlayer carbonate anion, and eventually the dehydroxylation of hydroxides taking place in the zone of 250-500°C [67]. Even if the presence of carbonate anion due the regeneration of the crystalline structure of LDH have been highlighted by various authors during the surface modification [68, 69]. The presence of imidazolium ionic liquids was clearly detected by TGA where the degradation peak at 370°C corresponds to the physically absorbed ionic liquids. In addition, the difference in the mass percentage between the LDH and the modified LDH indicates also the presence of the imidazolium ionic liquids.

Although XRD is a strong technic for evaluating the structure of LDH nanopalates, TEM is the most powerful evidence for describing the morphology of LDH in the epoxy nanocomposites. **Fig. 3** shows the TEM micrographs of LDH and LDH-IM in epoxy matrix at high (above) and low (below) magnifications. TEM images (**Fig. 3**) of the EP/LDH nanocomposites at high magnification reveals agglomerated LDH layers and dispersed layers are apparent from the TEM images of imidazolium- based ionic liquids modified LDH. As explained via XRD analysis, the basal spacing of LDH layers remain constant during modification when imidazolium cation physisorbed into LDH surface. Some black regions in low magnification TEM images illustrate the dispersibility state of nanopalates into epoxy matrix. As apparent, LDH nanopalates show weak dispersion and are highly agglomerated in the epoxy matrix. By contrast, imidazolium-

based IL-modified LDH is dispersed well into the epoxy system. The ionic liquid on the surface of LDH-IM acted as compatibilizing agents as well as dispersant leading to an appropriate dispersion of LDH-IM nanoplatelets into the epoxy compared to the LDH. The strong chemical interaction between imidazole groups of LDH-IM and epoxy rings dominates the tendency of LDH layers to agglomerate. Therefore, well-dispersed layers in epoxy are formed, which is shown by circles in TEM images.

3.2. Cure analysis

According to a protocol recommended for cure analysis of thermoset composites [57], the cure results of nonisothermal DSC at heating rates of 5, 10, and 15°C/min were analyzed in qualitative and quantitative manners. **Fig. 4** shows the DSC thermograms of the blank epoxy and its nanocomposites containing 0.1 mass% of LDH and LDH-IM as a function of heating rates. Observation of a single exothermic peak in DSC thermograms of all the samples confirmed the assumption of single step curing kinetic.

3.2.1. Qualitative cure analysis

Qualitative cure evaluation of epoxy nanocomposites containing 0.1 mass% of LDH and LDH-IM was performed by the *CI* [70]. The *CI* values for epoxy nanocomposites were calculated *via* the following equation:

$$CI = \Delta H^* \times \Delta T^* \quad (3)$$

The quantities of ΔH^* and ΔT^* were also calculated by the following **Eq. (4)** and **Eq. (5)**:

$$\Delta H^* = \frac{\Delta H_C}{\Delta H_{Ref}} \quad (4)$$

$$\Delta T^* = \frac{\Delta T_C}{\Delta T_{Ref}} \quad (5)$$

where ΔH_C and ΔH_{Ref} are the total enthalpy of cure for epoxy nanocomposites and the blank epoxy (the control of reference sample), respectively. In addition, ΔT_C and ΔT_{Ref} are the temperature intervals within which the cure of composites (EP/LDH or EP/LDH-IM) and EP are completed, respectively [71, 72]. The cure parameters including the values of ΔT^*, ΔH^* and the *CI* of blank and epoxy nanocomposites at heating rates of 5, 10 and 15°C/min are listed in **Table 2**. In addition, T_{Onset} and T_{Endset}, the onset and endset temperatures of the curing reaction, T_p as the maximum temperature of DSC peak, and ΔH_∞ as the heat of cure reaction are presented in **Table 2**.

Table 2. Cure characteristics of the prepared epoxy nanocomposites as a function of heating rate.

Designation	Heating rate (°C/min)	T_{Onset}(°C)	T_p(°C)	T_{Endset} (°C)	ΔT(°C)	ΔH_∞(J/g)	ΔT*	ΔH*	*CI*	*Cure state*
EP	5	45.00	92.00	209.00	164.00	303.95	n.a.	n.a.	n.a.	n.a.
	10	43.66	105.66	270.66	227.00	330.05	n.a.	n.a.	n.a.	n.a.
	15	42.30	114.30	292.30	250.00	372.70	n.a.	n.a.	n.a.	n.a.
EP/LDH	5	47.87	91.87	223.87	176.00	269.11	1.07	0.89	**0.95**	***Poor***
	10	44.51	105.51	240.51	196.00	255.77	0.86	0.77	**0.67**	***Poor***
	15	42.89	114.89	260.89	218.00	320.13	0.87	0.86	**0.75**	***Poor***
EP/LDH-IM	5	43.63	92.63	233.63	190.00	310.80	1.16	1.02	**1.18**	***Good***
	10	41.71	106.71	243.71	202.00	338.32	0.89	1.03	**0.91**	***Excellent***
	15	35.65	114.65	267.65	232.00	413.62	0.93	1.11	**1.03**	***Excellent***

n.a. – not applicable (reference measurements)

Mg-Al-CO_3 LDH resulted in increase of the onset cure temperature of epoxy regardless of the heating rate. By contrast, the presence of LDH-IM expedited the cure reaction, featured by a fall in the onset cure temperature. Moreover, analysis of changes in the values of ΔH_∞ revealed that LDH slowed down the cross-linking reaction due to the steric hindrance effect arising from large platelet-like nanoparticles that prevented interaction between epoxy and curing agent. However, imidazolium-based ionic liquid attached to the surface of LDH-IM provided epoxy resin additional help as the auxiliary curing agent that boosted epoxy curing reaction at elevated temperature. This can be attributed to the role of imidazole formed during the curing process at high temperature through thermal decomposition of ionic liquid structure [73, 74]. In addition, physisorbed ionic liquid acted as compatibilizing agents as well as dispersant aid leading to an appropriate dispersion of LDH-IM nanoplatelets into the epoxy compared to the LDH. The curing reaction between imidazole and epoxy featured by increase in the ΔH_∞ values with respect to neat epoxy was reported in several works [47, 75]. The possible reaction of imidazole with rings of epoxy resin is schematically shown in **Fig. 5**.

The cure state of epoxy nanocomposites including 0.1 mass% of Mg-Al-CO_3-LDH and LDH-IM has been graphically shown based on the *CI* in **Fig. S1** of supplementary information (SI). Addition of plate-like LDH into epoxy system resulted in *Poor* cure state (see **Table 2** or **Fig. S1**), indicating that plate-like nanoparticles hindered cross-linking of epoxy [76, 77]. By contrast, the accelerating and co-curing effects of imidazolium-based ionic liquid in the LDH-IM led to a shift from *Poor* to *Good* and *Excellent* in EP/LDH-IM system.

3.2.2. Quantitative cure analysis

3.2.2.1. Cure behavior

Cure conversion (α) can be calculated by using the following relation in which ΔH_T is the heat of reaction at a given temperature T:

$$\alpha = \frac{\Delta H_T}{\Delta H_\infty} \tag{6}$$

According to the sigmoidal shape of *α-time* curves obtained for EP, EP/LDH and EP/LDH-IM (see **Fig. S2** in the SI), the values of α increased slowly in the beginning of the curing reaction, while at the middle stage of cure when gelation occurred α increased rapidly and at late times became flat until the cure reaction completed. This phenomenon can be inferred on the ground of the acceleration role of the autocatalytic reaction by formation of OH intermediate products [5].

3.2.2.2. Cure kinetics

The rate of cure reaction in nonisothermal DSC depends on the $k(T)$ and $f(\alpha)$, respectively known as the reaction rate constant and reaction model, respectively:

$$\frac{d\alpha}{dt} = k(T) f(\alpha) \tag{7}$$

$k(T)$ is determined by Arrhenius equation:

$$k(T) = A \exp(-\frac{E_\alpha}{RT}) \tag{8}$$

In the **Eq. (8)** A, R, E_α and T are the frequency factor, universal gas constant, activation energy and the absolute temperature, respectively. By substituting **Eq. (8)** into **Eq. (7)** the curing rate can be rearranged to:

$$\frac{d\alpha}{dt} = A \exp(-\frac{E_\alpha}{RT}) f(\alpha) \tag{9}$$

The value of the activation energy can be obtained by isoconversional model-free methods. The differential isoconversional *Friedman* method is defined as follows [78]:

$$ln\left[\beta_i\left(\frac{d\alpha}{dT}\right)_{\alpha,i}\right]=ln[f(\alpha)A_\alpha]-\frac{E_\alpha}{RT_{\alpha,i}} \quad (10)$$

The *KAS* integral method is also defined as follows [79]:

$$ln\left(\frac{\beta_i}{T_{\alpha,i}^{1.92}}\right)=Const-1.0008\left(\frac{E_\alpha}{RT_\alpha}\right) \quad (11)$$

The variation of activation energy of epoxy nanocomposites was evaluated from nonisothermal DSC by isoconversional method in which the reaction rate at a given α is only dependent on the temperature [80]. The activation energy changes as a function of α are shown in **Fig. 6** (detailed procedure is represented in section S1.1 of the SI). Incorporation of the LDH and IM-modified LDH increased the activation energy of epoxy/amine systems due to the hindered effect of platelet-like LDH in curing moiety. Since LDH nanoplatelets cannot participate in curing reaction, they hindered cross-linking leading to an incomplete cure. In the case of EP/LDH-IM, since the imidazole formed during cure could participate in curing reaction as curing aid, the stoichiometry was changed by increasing the number of curing agents so that the number of curable molecules per unit volume was increased. As a result, reaction was continued when gelation occurred in the EP/LDH-IM system. Thus, the substantial increase in the value of activation energy of the assigned system compared to the neat epoxy and EP/LDH was the result of excessive collision in the system.

To determine the reaction model ($f(\alpha)$) of the prepared samples, *Friedman* and *Malek* [81, 82] methods were chosen for recognizing the noncatalytic and autocatalytic reactions. The details of *Friedman* and *Malek* methods and their mathematical formulas are provided in section S1.2 of SI, where **Fig. S4** to **Fig. S7** can be considered for meticulous analysis. Two-parameter autocatalytic kinetic model was confirmed for epoxy, epoxy/LDH and epoxy/LDH-IM systems

by *Friedman* and *Malek* methods. Two-parameter autocatalytic kinetic model was defined by Sestak-Berggren as follows:

$$f(\alpha)=\alpha^{m}(1-\alpha)^{n} \quad (12)$$

The degrees of autocatalytic reaction (*m* and *n*) and the pre-exponential factor (*LnA*) were calculated based on *Malek* (as mentioned in section S1.2 of SI file). The parameters of *Friedman* and *KAS* methods are listed in **Table 3**. As the curing reaction of the prepared samples is on the basis of autocatalysis reaction, it is expected that the values of *m* and *n* change for each value of conversion. Therefore, we considered time-dependent orders of reactions to find the values of *m* and *n* based on *Friedman* and *KAS* methods at each conversion by using the iteration method through minimizing the difference between the experimental and theoretical values of *dα/dt* for certain values of conversion (i.e. 0.1, 0.2, ..., 0.9).

Table 3. The kinetic parameters evaluated for the curing of pristine epoxy resin and its nanocomposites based on *Malek*, *Friedman* and *KAS* models at different heating rates

Designation	Heating rate (°C/min)	$\bar{E}_\alpha$ (kJ/mol)	*Ln(A)* (1/s)	Mean (1/s)	*m*	Mean	*n*	Mean
Malek								
EP	5	61.20	19.82	19.68	0.142	0.120	2.139	2.227
	10		19.77		0.187		2.282	
	15		19.44		0.030		2.259	
EP/LDH	5	63.24	21.28	21.15	0.115	0.099	1.961	2.018
	10		21.13		0.101		1.913	
	15		21.04		0.082		2.179	
EP/LDH-IM	5	67.47	23.49	23.36	0.069	0.040	2.315	2.311
	10		23.45		0.045		2.159	
	15		23.14		0.007		2.458	
Friedman								
Epoxy	5	44.73	13.28	13.41	0.228	0.264	1.624	1.780

	10		13.44		0.299		1.796	
	15		13.50		0.265		1.920	
EP/LDH	5	47.47	13.90	14.17	0.079	0.176	1.382	1.553
	10		14.25		0.215		1.508	
	15		14.36		0.233		1.770	
EP/LDH-IM	5	49.48	14.75	14.93	0.169	0.223	1.681	1.702
	10		15.06		0.257		1.614	
	15		14.96		0.241		1.812	
KAS								
Epoxy	5	64.65	19.80	19.72	0.030	0.048	2.056	2.157
	10		19.73		0.064		2.166	
	15		19.63		0.049		2.250	
EP/LDH	5	66.68	20.15	20.24	0.133	0.061	1.634	1.818
	10		20.28		0.012		1.771	
	15		20.28		0.040		2.048	
EP/LDH-IM	5	71.63	21.98	21.94	0.066	0.057	1.992	2.055
	10		22.07		0.029		1.969	
	15		21.77		0.074		2.205	

The overall orders of cure reaction ($m+n$) for the neat epoxy and epoxy/LDH nanocomposites are larger than one, which suggest the complexity of curing of the studied epoxy/amine systems. The autocatalytic reaction order (m) was decreased by the incorporation of LDH into epoxy resin, signifying a change in the curing reaction mechanism from autocatalytic to noncatalytic reaction. This phenomenon is due to the hindrance effect of platy like LDH on the curing of cure moiety.

The validity of *Friedman* and *KAS* models is evaluated by comparison of the curves of calculated $d\alpha/dt$ as a function of T plotted with the experimental data. We also compared the results for EP, EP/LDH and EP/LDH-IM in **Fig. S8** of S1.3 in the SI. It can be observed that calculated data from *Friedman* and *KAS* models coincides well with experimental data.

3.3. Surface energy

The surface free energy components for the neat epoxy and its nanocomposites were calculated and reported in **Table 4**. The total surface free energy is divided into two components of non-dispersive (polar) and dispersive components, where γ^L is the London dispersive component and the γ^{SP} is the specific (or polar) component. The polar component of EP/LDH system was increased compared to that of neat epoxy system. However, EP/LDH-IM remained almost unchanged. Substitution of the hydrogen atoms on the surface of LDH by imidazolium-based ionic liquid, an increase in the dispersion force component was achieved. Large hydrogen-bonding ability of EP/LDH system may be attributed to the incomplete epoxy network formation due to the hindrance effect of platelet-like LDH. Higher γ_S^{SP} component of the surface free energy of EP/LDH than that of neat epoxy is due to the weak intramolecular hydrogen bonding [83].

Table 4. The surface free energy components of neat epoxy and its nanocomposites

Samples	γ_S^L	γ_S^{SP}	γ_S
EP	34.2	2.8	37.0
EP/LDH	25.5	12.4	37.9
EP/LDH-IM	34.9	3.3	38.0

3.4. Viscoelastic behavior assessment

Viscoelastic behavior of the neat epoxy, EP/LDH and EP/LDH-IM was studied by temperature-sweep dynamic mechanical measurements at frequency of 1 Hz. In this manner, the dynamic properties of epoxy in the presence of 0.1 mass% of LDH and LDH-IM was uncovered. The dynamic properties reflected the alteration of energy in the system stored as the elastic energy and the energy dissipated during the strain process. The important parameters affecting the

dynamic properties in a nanocomposite are the dispersion state of nanoparticles in the matrix, volume fraction of particles, their geometry, functionality and load transfer between the nanoparticles and the matrix [84, 85]. The dynamic storage modulus (E′), loss modulus (E") and tan δ curves as a function of temperature for the neat epoxy, EP/LDH and EP/LDH-IM are shown in **Fig. 7**. It is clear that both epoxy nanocomposites containing 0.1 mass% of LDH and LDH-IM have higher E′ (around 70% increment) at the glassy region compared to the neat epoxy. In the vicinity of the glass transition area, E" for all the samples shows an abrupt plummet. This transition occurred for EP/LDH, neat epoxy and EP/LDH-IM from low to the high temperatures in the mentioned order, indicating that positive effects of surface modification of LDH nanopalates with imidazolium ionic liquid on network formation of epoxy resulted in enhancement of crosslinking density of the epoxy system, which were dominant compared to the hindrance effect of LDH on the curing reactions of epoxy resin. These results are in agreement with the *CI* values highlighted in previous section which represented *Good* and *Excellent* cure state for EP/LDH-IM nanocomposites against *Poor* cure state suggested for EP/LDH system. At temperatures well above the glass transition region, the E′ reached a plateau in the rubbery stage, which is magnified in **Fig. 7**. The higher E′ value of the EP/LDH-IM system in the rubbery region is an indication of increased crosslink density of epoxy resin in the presence of LDH-IM due to the reaction of imidazole formed during the thermal decomposition of ionic liquid structure.

The peaks in the plots of tanδ are indicative of glass transition temperatures. The T_g values are measured by DMA are compared with those measured by DSC (see **Table 5**). The T_g values that are measured using DMA and DSC methods are not the same, due to the fact that each technique works on the basis of a different physical phenomenon, which leads to a significant change in the

glass transition. The glass transition measured using DSC is based on the change in the heat capacity, while in the DMA a change in the mechanical properties of storage or loss modulus is detected for calculating T_g [86].

The T_g values based on DSC were obtained at heating rates of 5, 10, 15°C/min of fully cured neat epoxy and its nanocomposites containing 0.1 mass% of LDH and LDH-IM. It is obvious that there is a fall in T_g upon addition of LDH based on both DSC and DMA methods. The variation of T_g reflects the ease of polymer chains to relax and can be considered as an evidence of interactions between the reinforcing phase (nanoparticles) and the polymeric matrix [87, 88]. The decrease in the T_g of EP/LDH nanocomposite with respect to the blank epoxy denotes weak interactions between the LDH platelet-like nanoparticles and epoxy matrix. By contrast, with addition of LDH-IM a higher T_g value was observed compared to the blank epoxy resin, indicating a reduction in the segmental mobility of polymer chains. This indicated that, LDH-IM can create strong interactions with epoxy matrix as proved by the *CI*, which showed *Good* and *Excellent* cure state.

Table 5. Glass transition temperature of the fully cured EP, EP/LDH and EP/LDH-IM

Designation	T_g (°C)	
	DMA	**DSC**
EP	94.1	89.2
EP/LDH	82.1	81.7
EP/LDH-IM	96.6	93.4

3.5. TGA of nanocomposites

3.5.1. Thermal stability of nanocomposites

Thermal degradation of the neat epoxy and its nanocomposites containing 0.5, 2 and 5 mass% of LDH and LDH-IM nanoplatelets were studied by TGA. **Fig. 8** shows TGA and DTG of the prepared samples. Thermal degradation parameters such as T_5 and T_P which represent decomposition temperature of 5% and peak mass loss, respectively and char residue at the end of TGA test are extracted and reported in **Table 6**.

The temperature of the EP/LDH and EP/LDH-IM for the mass loss of 5% was higher than that of neat epoxy. Addition of LDH and LDH-IM to the epoxy matrix reduced the mobility of the epoxy chain around the nanopalates and enhanced thermal stability. The increase of T_5 in the case of EP/LDH-IM nanocomposites is lower than that of EP/LDH due to the decomposition of the organic species physically adsorbed onto the surface of LDH. However, the T_P of the nanocomposites remained unaffected with respect to the neat epoxy. The degradation of EP/LDH-IM exhibited a higher value of the char residue compared to the other samples because of carbon formation in the epoxy system [89].

Table 6. Thermal degradation parameters of neat epoxy and its nanocomposites.

Designation	T_5 (°C)	T_P (°C)	Residue (%) at 900 °C
EP	162.09	371.95	10.90
EP/LDH-0.5	171.66	369.52	11.33
EP/LDH-2	166.92	369.20	11.66
EP/LDH-5	164.12	365.89	13.11
EP/LDH-IM-0.5	165.92	370.83	9.33
EP/LDH-IM-2	161.87	370.60	7.44
EP/LDH-IM-5	201.32	365.14	15.17

3.5.2. Decomposition kinetics

The conversion of the decomposition (α) is defined as follows [90]:

$$\alpha = \frac{(W_0 - W_t)}{(W_0 - W_f)}$$

(13)

where W_0, W_t and W_f are the initial mass, polymer mass at time t and the final mass of polymer at the end of decomposition. The profiles of conversion of the decomposition for neat epoxy ant its nanocomposites containing 0.5, 2 and 5 mass% of LDH and LDH-IM at different heating rates are shown in **Fig. S9** (section S2 of SI). By increasing the heating rate the degradation conversion shifted to higher temperatures and the pyrolysis process became faster due to the restricted time [91].

KAS isoconversional method was considered for predicting the activation energy of the degradation reaction of neat epoxy and its nanocomposites containing 0.5, 2 and 5 mass% of LDH and LDH-IM. **Fig. 9** shows the evolution of decomposition activation energy as a functional of α based on *KAS* method (the details can be find in section S2.1 of SI file) for the neat epoxy and its nanocomposites containing 0.5, 2 and 5 mass% of LDH and LDH-IM. At first, the E_α values of jumped abruptly and then reached to a near flat region. Finally, a gradual rise in E_α values can be observed. Independent on the isoconversional method, activation energy of nanocomposites increased in comparison with neat epoxy. As apparent, the activation energy values increased with increasing LDH and LDH-IM content from 0.5 to 5 mass%. Epoxy system containing 5 mass% of LDH-IM shows highest E_α values due to the presence of higher amount of thermally stable LDH nanopalates with imidazolium- based IL on their surface. The imidazole of IL on the surface of LDH can interact with epoxy resin and results in denser network which makes the decomposition reaction more difficult and leads to higher activation energy.

The reaction model $f(\alpha)$ was determined with the help of Criados master plots [92], expression:

$$\frac{Z(\alpha)}{Z(0.5)} = \frac{f(\alpha)g(\alpha)}{f(0.5)g(0.5)} = \left(\frac{T_\alpha}{T_{0.5}}\right)^2 \frac{(d\alpha/dt)_\alpha}{(d\alpha/dt)_{0.5}} \quad (14)$$

The Criado method compares experimental TGA results with the frequently used reaction models and associated functions, *f(α)* and *g(α)*, as tabulated in **Table 7**.

Table 7. Reaction models of most common reaction mechanism considered in solid-state reactions [80, 93].

Reaction Model	Model Code	*f(α)*	*g(α)*
Power law	P2	$2\alpha^{1/2}$	$\alpha^{1/2}$
Power law	P3	$3\alpha^{2/4}$	$\alpha^{1/3}$
Power law	P4	$4\alpha^{3/4}$	$\alpha^{1/4}$
Avrami-Erofeev: Two-dimensional nucleation	A2	$2(1-\alpha)[-\ln(1-\alpha)]^{1/2}$	$[-\ln(1-\alpha)]^{1/2}$
Avrami-Erofeev: Three-dimensional nucleation	A3	$3(1-\alpha)[-\ln(1-\alpha)]^{2/4}$	$[-\ln(1-\alpha)]^{1/3}$
Avrami-Erofeev: Four-dimensional nucleation	A4	$4(1-\alpha)[-\ln(1-\alpha)]^{3/4}$	$[-\ln(1-\alpha)]^{1/4}$
Contracting cylinder: Two dimensional phase boundary reaction	R2	$2(1-\alpha)^{1/2}$	$1-(1-\alpha)^{1/2}$
Contracting sphere: Three dimensional phase boundary reaction	R3	$3(1-\alpha)^{2/3}$	$1-(1-\alpha)^{1/3}$
Two-dimensional diffusion	D2	$[-\ln(1-\alpha)]^{-1}$	$(1-\alpha)\ln(1-\alpha)+\alpha$
Three dimensional diffusion	D3	$3/2(1-\alpha)^{2/3}[1-(1-\alpha)^{1/3}]^{-1}$	$[1-(1-\alpha)^{1/3}]^2$
Mampel (first order)	F1	$1-\alpha$	$-\ln(1-\alpha)$
One-dimensional diffusion	D1	$1/2\alpha^{-1}$	α^2
Ginstling-Brounshtein	D4	$3/2((1-\alpha)^{-1/3}-1)$	$1-(2\alpha/3)-(1-\alpha)^{2/3}$
Second order	F2	$(1-\alpha)^2$	$(1-\alpha)^{-1}-1$
Third order	F3	$(1-\alpha)^3$	$[(1-\alpha)^{-1}-1]/2$

where $T_{0.5}$ and $(d\alpha/dt)_{0.5}$ represent the temperature and the rate of degradation at $\alpha = 0.5$. The left-hand side $[(f(\alpha)g(\alpha))/f(0.5)g(0.5)]$ of **Eq. (14)** represents the theoretical master plots obtained

from each reaction mechanism mentioned in **Table 7**. The right-hand side of **Eq. (14)** was calculated from the experimental results. Comparing the theoretical master plots with those obtained experimentally, the most suitable reaction model was obtained. The theoretical master plots of $z(\alpha)/z(0.5)$ as a function of α for different mechanisms (**Table 7**) along with experimental reduced plots for the neat epoxy and its nanocomposites are illustrated in **Fig. 10** at a heating rate of 5 ˚C/min. The reaction model for a system of multiple complex reactions has little meaning, yet the reaction model was predicted to comprehend the apparent reaction model. Apparent from **Fig. 10**, the degradation kinetic models for EP, EP/LDH-0.5, EP/LDH-2, EP/LDH-5, EP/LDH-IM-0.5, EP/LDH-IM-2 and EP/LDH-IM-5 were found to be D4, D2, A3, F2, A2 and D3 for the conversion values from 0.2 to 0.4, respectively. The data was fitting with F3 model for conversion values in the range of 0.5-0.8.

Sestak and Berggren (**Eq. (12)**) proposed an empirical function that permits accommodation of a wide range of real changes described by an $f(\alpha)$ function. **Table 8** reports the decomposition kinetic parameters of Sestak-Berggren function of neat epoxy and its nanocomposites based on the *KAS* isoconversional method. The decomposition reaction order ($n+m$) increased by the addition of LDH and LDH-IM nanopalates to the epoxy matrix, suggesting that the rate of decomposition reaction decreased with introduction of nanoparticles. The frequency factor (LnA) significantly rose by adding LDH and LDH-IM and their content in the epoxy matrix, which is obvious in the case of EP/LDH-IM nanocomposites. Introduction of LDH-IM made thermal decomposition reaction difficult due to the formation of denser epoxy network as a result of chemical interactions between imidazolium-based ionic liquid in the LDH-IM structure and epoxy resin. Strong interfacial adhesion in the region near LDH-IM and epoxy matrix hindered

the molecular motion and led to dissipating more energy, which resulted in higher resistant against thermal decomposition.

Table 8. Decomposition parameters of epoxy and its nanocomposites using *KAS* isoconversional kinetic model.

Designation	E_α (kJ/mol)	LnA (min^{-1})	m	n
E0	124.0	20.7	1.1	1.1
E-LDH-0.5	129.7	25.0	1.2	2.6
E-LDH-2	192.7	37.2	1.0	3.3
E-LDH-5	191.7	35.6	0.9	3.1
E-LDH-IM-0.5	150.2	29.5	1.5	3.3
E-LDH-IM-2	128.0	22.4	1.1	2.2
E-LDH-IM-5	181.6	33.3	0.8	2.1

The experimental and model predicted decomposition reaction rate based on the Sestak and Berggren model for neat epoxy and its nanocomposites using *KAS* isoconversional method is shown in **Fig. S11** (section S2.2 of SI). *KAS* method represents good correlation with the experimental and have similar decomposition trend.

Conclusion

In this work, Mg-Al-CO_3-LDH modified by imidazoline ionic liquid and modification was proved by XRD and TGA analyses. Besides, epoxy nanocomposite was prepared by 0.1, 0.5, 2 and 5 mass% of LDH and LDH-IM. TEM denoted the effect of imidazolium- based IL on intercalation of LDH layers and indicated appropriate dispersion state of LDH-IM in epoxy matrix. The qualitative cure analysis of EP, EP/LDH and EP/LDH-IM was evaluated by nonisothermal DSC analysis. According to the *CI* values EP/LDH showed the *Poor* cure state due to the hindrance effect of plate-like LDH particles. While imidazole-based ionic liquid

modified LDH shifted the cure state to the *Good* at low heating rate (β=5°C/min) and *Excellent* at β of 10 and 15°C/min thanks to facilitation effect of imidazole groups in epoxide ring opening. It was also revealed that the activation energy for epoxy system increases respect to neat epoxy due to the hindrance effect of platelet-like LDH. Higher polar component of surface free energy of EP/LDH than the neat epoxy system is indicated the weak intramolecular hydrogen bonding. The higher storage modulus value of the EP/LDH-IM-0.1 system in the rubbery region is indication of increasing crosslink density of epoxy resin due to the reaction of imidazole of IL structure with epoxy ring. The decrement of T_g for EP/LDH nanocomposite by both DMA and DSC methods denotes weak interactions between LDH plate-like particles and epoxy matrix. While, LDH-IM increased T_g of epoxy system (96.6°C from DMA and 93.4°C from DSC) compared to neat epoxy (94.1°C from DMA and 89.2°C from DSC) which is attributed to the strong interactions between LDH-IM and epoxy matrix. The *KAS* isoconversional method represented the rise in decomposition activation energy and frequency factor values by addition of LDH-IM in epoxy matrix especially in 5 mass% which indicated the strong interfacial surface in the vicinity of LDH-IM and epoxy matrix that hardened the molecular motion and consequently thermal decomposition.

References

[1] J.H. Hodgkin, G.P. Simon, R.J. Varley, Thermoplastic toughening of epoxy resins: a critical review, Polymers for Advanced Technologies, 9 (1998) 3-10.
[2] R. Mezzenga, L. Boogh, J.-A.E. Månson, A review of dendritic hyperbranched polymer as modifiers in epoxy composites, Composites Science and Technology, 61 (2001) 787-795.
[3] M. Jouyandeh, M.R. Ganjali, J.A. Ali, M. Aghazadeh, S.M.R. Paran, G. Naderi, M.R. Saeb, S. Thomas, Curing epoxy with polyvinylpyrrolidone (PVP) surface-functionalized ZnxFe3-xO4 magnetic nanoparticles, Progress in Organic Coatings, 136 (2019) 105227.
[4] S. Zheng, D.A. Bellido-Aguilar, Y. Huang, X. Zeng, Q. Zhang, Z. Chen, Mechanically robust hydrophobic bio-based epoxy coatings for anti-corrosion application, Surface and Coatings Technology, 363 (2019) 43-50.

[5] H. Vahabi, M. Jouyandeh, M. Cochez, R. Khalili, C. Vagner, M. Ferriol, E. Movahedifar, B. Ramezanzadeh, M. Rostami, Z. Ranjbar, B.S. Hadavand, M.R. Saeb, Short-lasting fire in partially and completely cured epoxy coatings containing expandable graphite and halloysite nanotube additives, Progress in Organic Coatings, 123 (2018) 160-167.
[6] M. Jouyandeh, J.A. Ali, V. Akbari, M. Aghazadeh, S.M.R. Paran, G. Naderi, M.R. Saeb, Z. Ranjbar, M.R. Ganjali, Curing epoxy with polyvinylpyrrolidone (PVP) surface-functionalized MnxFe3-xO4 magnetic nanoparticles, Progress in Organic Coatings, 136 (2019) 105247.
[7] M. Jouyandeh, F. Tikhani, N. Hampp, D. Akbarzadeh Yazdi, P. Zarrintaj, M. Reza Ganjali, M. Reza Saeb, Highly curable self-healing vitrimer-like cellulose-modified halloysite nanotube/epoxy nanocomposite coatings, Chemical Engineering Journal, 396 (2020) 125196.
[8] M. Lee, W. Kwon, D. Kwon, E. Lee, E. Jeong, Fracture toughness of the novel in-situ polytriazolesulfone modified epoxy resin for carbon fiber/epoxy composites, Journal of Industrial and Engineering Chemistry, 77 (2019) 461-469.
[9] N. Chikhi, S. Fellahi, M. Bakar, Modification of epoxy resin using reactive liquid (ATBN) rubber, European Polymer Journal, 38 (2002) 251-264.
[10] R. Thomas, D. Yumei, H. Yuelong, Y. Le, P. Moldenaers, Y. Weimin, T. Czigany, S. Thomas, Miscibility, morphology, thermal, and mechanical properties of a DGEBA based epoxy resin toughened with a liquid rubber, Polymer, 49 (2008) 278-294.
[11] M. Jouyandeh, E. Yarahmadi, K. Didehban, S. Ghiyasi, S.M.R. Paran, D. Puglia, J.A. Ali, A. Jannesari, M.R. Saeb, Z. Ranjbar, M.R. Ganjali, Cure kinetics of epoxy/graphene oxide (GO) nanocomposites: Effect of starch functionalization of GO nanosheets, Progress in Organic Coatings, (2019) 105217.
[12] B. Zhang, Y. Zhao, X. Sun, X. Fei, W. Wei, X. Li, X. Liu, Microcapsules derived from Pickering emulsions as thermal latent curing accelerator for epoxy resins, Journal of Industrial and Engineering Chemistry, 83 (2020) 224-234.
[13] F. Seidi, M. Jouyandeh, M. Taghizadeh, A. Taghizadeh, H. Vahabi, S. Habibzadeh, K. Formela, M.R. Saeb, Metal-Organic Framework (MOF)/Epoxy Coatings: A Review, Materials, 13 (2020) 2881.
[14] S. Kango, S. Kalia, A. Celli, J. Njuguna, Y. Habibi, R. Kumar, Surface modification of inorganic nanoparticles for development of organic–inorganic nanocomposites—A review, Progress in Polymer Science, 38 (2013) 1232-1261.
[15] M. Jouyandeh, S.M.R. Paran, M. Shabanian, S. Ghiyasi, H. Vahabi, M. Badawi, K. Formela, D. Puglia, M.R. Saeb, Curing behavior of epoxy/Fe 3 O 4 nanocomposites: A comparison between the effects of bare Fe 3 O 4, Fe 3 O 4/SiO 2/chitosan and Fe 3 O 4/SiO 2/chitosan/imide/phenylalanine-modified nanofillers, Prog. Org. Coat., 123 (2018) 10-19.
[16] F. Seidi, M. Jouyandeh, A. Taghizadeh, M. Taghizadeh, S. Habibzadeh, Y. Jin, H. Xiao, P. Zarrintaj, M.R. Saeb, Polyhedral Oligomeric Silsesquioxane (POSS)/Epoxy Coatings: A Review, Surface Innovations, (2020) 1-11.
[17] M. Jouyandeh, P. Zarrintaj, M.R. Ganjali, J.A. Ali, I. Karimzadeh, M. Aghazadeh, M. Ghaffari, M.R. Saeb, Curing epoxy with electrochemically synthesized GdxFe3-xO4 magnetic nanoparticles, Progress in Organic Coatings, 136 (2019) 105245.
[18] T.A. Truc, T.T. Thuy, V.K. Oanh, T.T.X. Hang, A.S. Nguyen, N. Caussé, N. Pébère, 8-hydroxyquinoline-modified clay incorporated in an epoxy coating for the corrosion protection of carbon steel, Surfaces and Interfaces, 14 (2019) 26-33.
[19] Z. Karami, M. Jouyandeh, J.A. Ali, M.R. Ganjali, M. Aghazadeh, M. Maadani, M. Rallini, F. Luzi, L. Torre, D. Puglia, V. Akbari, M.R. Saeb, Cure Index for labeling curing potential of

epoxy/LDH nanocomposites: A case study on nitrate anion intercalated Ni-Al-LDH, Progress in Organic Coatings, 136 (2019) 105228.
[20] F.R. Costa, M. Saphiannikova, U. Wagenknecht, G. Heinrich, Layered double hydroxide based polymer nanocomposites, Wax Crystal Control· Nanocomposites· Stimuli-Responsive Polymers, Springer2007, pp. 101-168.
[21] Z. Karami, M. Jouyandeh, J.A. Ali, M.R. Ganjali, M. Aghazadeh, S.M.R. Paran, G. Naderi, D. Puglia, M.R. Saeb, Epoxy/layered double hydroxide (LDH) nanocomposites: Synthesis, characterization, and Excellent cure feature of nitrate anion intercalated Zn-Al LDH, Prog. Org. Coat., 136 (2019) 105218.
[22] J. Wei, J. Xu, Y. Mei, Q. Tan, Chloride adsorption on aminobenzoate intercalated layered double hydroxides: Kinetic, thermodynamic and equilibrium studies, Applied Clay Science, 187 (2020) 105495.
[23] T. Kameda, M. Takaizumi, S. Kumagai, Y. Saito, T. Yoshioka, Adsorption of various metals by carboxymethyl-β-cyclodextrin-modified ZnAl layered double hydroxides, Applied Clay Science, 187 (2020) 105479.
[24] T. Hibino, Deterioration of anion-adsorption abilities of layered double hydroxides synthesized in agarose gel, Applied Clay Science, 186 (2020) 105435.
[25] F. Pazoki, M. Shamsayei, S. Bagheri, E. Yazdani, A. Heydari, MnO2@Mg-Al layered double hydroxide Nanosheets: A sustainable and recyclable photocatalyst toward oxidation of benzyl alcohol, Applied Clay Science, 187 (2020) 105494.
[26] S. Li, Y. Yang, S. Huang, Z. He, C. Li, D. Li, B. Ke, C. Lai, Q. Peng, Adsorption of humic acid from aqueous solution by magnetic Zn/Al calcined layered double hydroxides, Applied Clay Science, (2020) 105414.
[27] H. Palza, K. Delgado, J. Govan, Novel magnetic CoFe2O4/layered double hydroxide nanocomposites for recoverable anionic adsorbents for water treatment, Applied Clay Science, 183 (2019) 105350.
[28] Y. Wang, H. Gao, Compositional and structural control on anion sorption capability of layered double hydroxides (LDHs), Journal of colloid and interface science, 301 (2006) 19-26.
[29] S.R. Tavares, C. Carvalho, K.M. Mantovani, F. Wypych, S. Nakagaki, A.A. Leitão, Adsorption of an iron(III)porphyrin onto a 2:1 Zn/Al-CO3 layered double hydroxide and its use as an oxidation catalyst with different counter ions: An experimental and DFT study, Applied Clay Science, 185 (2020) 105410.
[30] C.M. Becker, A.D. Gabbardo, F. Wypych, S.C. Amico, Mechanical and flame-retardant properties of epoxy/Mg–Al LDH composites, Composites Part A: Applied Science and Manufacturing, 42 (2011) 196-202.
[31] B. Li, Y. Hu, Z. Chen, W. Fan, Preparation for a new intercalated compound of acrylamide monomers and their in-situ polymerization in layered double hydroxides, Materials Letters, 61 (2007) 2761-2764.
[32] E.N. Kalali, X. Wang, D.-Y. Wang, Multifunctional intercalation in layered double hydroxide: toward multifunctional nanohybrids for epoxy resin, J. Mater. Chem A., 4 (2016) 2147-2157.
[33] J.I. Velasco, M. Ardanuy, M. Antunes, 4 - Layered double hydroxides (LDHs) as functional fillers in polymer nanocomposites, in: F. Gao (Ed.) Advances in Polymer Nanocomposites, Woodhead Publishing2012, pp. 91-130.
[34] W. Chen, B. Qu, LLDPE/ZnAl LDH-exfoliated nanocomposites: effects of nanolayers on thermal and mechanical properties, Journal of Materials Chemistry, 14 (2004) 1705-1710.

[35] Y. Yuan, W. Shi, Preparation and properties of exfoliated nanocomposites through intercalated a photoinitiator into LDH interlayer used for UV curing coatings, Progress in Organic Coatings, 69 (2010) 92-99.
[36] K. Zhou, R. Gao, X. Qian, Self-assembly of exfoliated molybdenum disulfide (MoS2) nanosheets and layered double hydroxide (LDH): Towards reducing fire hazards of epoxy, Journal of Hazardous Materials, 338 (2017) 343-355.
[37] P.K. Kaul, A.J. Samson, G.T. Selvan, I. Enoch, P.M. Selvakumar, Synergistic effect of LDH in the presence of organophosphate on thermal and flammable properties of an epoxy nanocomposite, Applied Clay Science, 135 (2017) 234-243.
[38] Y. Su, S. Qiu, D. Yang, S. Liu, H. Zhao, L. Wang, Q. Xue, Active anti-corrosion of epoxy coating by nitrite ions intercalated MgAl LDH, Journal of Hazardous Materials, 391 (2020) 122215.
[39] J. Ding, Y. Zhang, X. Zhang, Q. Kong, J. Zhang, H. Liu, F. Zhang, Improving the flame-retardant efficiency of layered double hydroxide with disodium phenylphosphate for epoxy resin, Journal of Thermal Analysis and Calorimetry, (2019) 1-8.
[40] Y.-N. Chan, T.-Y. Juang, Y.-L. Liao, S.A. Dai, J.-J. Lin, Preparation of clay/epoxy nanocomposites by layered-double-hydroxide initiated self-polymerization, Polymer, 49 (2008) 4796-4801.
[41] H. Rastin, M.R. Saeb, M. Nonahal, M. Shabanian, H. Vahabi, K. Formela, X. Gabrion, F. Seidi, P. Zarrintaj, M.G. Sari, P. Laheurte, Transparent nanocomposite coatings based on epoxy and layered double hydroxide: Nonisothermal cure kinetics and viscoelastic behavior assessments, Progress in Organic Coatings, 113 (2017) 126-135.
[42] Z. Karami, M. Jouyandeh, J.A. Ali, M.R. Ganjali, M. Aghazadeh, M. Maadani, M. Rallini, F. Luzi, L. Torre, D. Puglia, V. Akbari, M.R. Saeb, Cure Index for labeling curing potential of epoxy/LDH nanocomposites: A case study on nitrate anion intercalated Ni-Al-LDH, Progress in Organic Coatings, (2019) 105228.
[43] Z. Karami, M. Jouyandeh, S. Ghiyasi, J.A. Ali, M.R. Ganjali, M. Aghazadeh, M. Maadani, M. Rallini, F. Luzi, L. Torre, D. Puglia, M.R. Saeb, Exploring curing potential of epoxy nanocomposites containing nitrate anion intercalated Mg–Al–LDH with Cure Index, Prog. Org. Coat., 139 (2020) 105255.
[44] Z. Karami, M. Aghazadeh, M. Jouyandeh, P. Zarrintaj, H. Vahabi, M.R. Ganjali, L. Torre, D. Puglia, M.R. Saeb, Epoxy/Zn-Al-CO3 LDH nanocomposites: Curability assessment, Prog. Org. Coat., 138 (2020) 105355.
[45] X. Yang, J. Zhu, D. Yang, J. Zhang, Y. Guo, X. Zhong, J. Kong, J. Gu, High-efficiency improvement of thermal conductivities for epoxy composites from synthesized liquid crystal epoxy followed by doping BN fillers, Composites Part B: Engineering, 185 (2020) 107784.
[46] K. Matsumoto, T. Endo, Confinement of Ionic Liquid by Networked Polymers Based on Multifunctional Epoxy Resins, Macromolecules, 41 (2008) 6981-6986.
[47] S. Huo, S. Yang, J. Wang, J. Cheng, Q. Zhang, Y. Hu, G. Ding, Q. Zhang, P. Song, A liquid phosphorus-containing imidazole derivative as flame-retardant curing agent for epoxy resin with enhanced thermal latency, mechanical, and flame-retardant performances, Journal of Hazardous Materials, 386 (2020) 121984.
[48] D.F. Santos, A.P.A. Carvalho, B.G. Soares, Phosphonium-based ionic liquid as crosslinker/dispersing agent for epoxy/carbon nanotube nanocomposites: electrical and dynamic mechanical properties, Journal of Materials Science, 55 (2020) 2077-2089.

[49] A. Khalili Dermani, E. Kowsari, B. Ramezanzadeh, R. Amini, Utilizing imidazole based ionic liquid as an environmentally friendly process for enhancement of the epoxy coating/graphene oxide composite corrosion resistance, Journal of Industrial and Engineering Chemistry, 79 (2019) 353-363.
[50] S. Livi, G. Sar, V. Bugatti, E. Espuche, J. Duchet-Rumeau, Synthesis and physical properties of new layered silicates based on ionic liquids: improvement of thermal stability, mechanical behaviour and water permeability of PBAT nanocomposites, RSC advances, 4 (2014) 26452-26461.
[51] G.K. Dedzo, Kaolinite Clay Mineral Reactivity Improvement through Ionic Liquid Functionalization, Israel Journal of Chemistry, 59 (2019) 778-788.
[52] O. Alekseeva, A. Noskov, E. Grishina, L. Ramenskaya, N. Kudryakova, V. Ivanov, A. Agafonov, Structural and Thermal Properties of Montmorillonite/Ionic Liquid Composites, Materials, 12 (2019) 2578.
[53] F. Xiao, B.-q. Yan, X.-y. Zou, X.-q. Cao, L. Dong, X.-j. Lyu, L. Li, J. Qiu, P. Chen, S.-g. Hu, Study on ionic liquid modified montmorillonite and molecular dynamics simulation, Colloids and Surfaces A: Physicochemical and Engineering Aspects, 587 (2020) 124311.
[54] H. Lyu, Y. Ling, J. Fan, Y. Chen, Y. Yu, Z. Xie, Preparation of ionic liquid-functionalized layered double hydroxide via thiol-ene click chemistry for highly efficient removal of azo dyes during broad pH range, Journal of cleaner production, 211 (2019) 1026-1033.
[55] S. Bujok, M. Konefał, S. Abbrent, E. Pavlova, J. Svoboda, O. Trhlikova, Z. Walterova, H. Beneš, Ionic liquid-functionalized LDH as catalytic-initiating nanoparticles for microwave-activated ring opening polymerization of ε-caprolactone, Reaction Chemistry & Engineering, (2020).
[56] S. Livi, V. Bugatti, L. Estevez, J. Duchet-Rumeau, E.P. Giannelis, Synthesis and physical properties of new layered double hydroxides based on ionic liquids: Application to a polylactide matrix, Journal of Colloid and Interface Science, 388 (2012) 123-129.
[57] M. Jouyandeh, M.R. Ganjali, J.A. Ali, M. Aghazadeh, F.J. Stadler, M.R. Saeb, Curing epoxy with electrochemically synthesized CoxFe3-xO4 magnetic nanoparticles, Progress in Organic Coatings, 137 (2019) 105252.
[58] S. Livi, J. Duchet-Rumeau, J.F. Gérard, Effect of ionic liquid modified synthetic layered silicates on thermal and mechanical properties of high density polyethylene nanocomposites, Macromolecular Symposia, Wiley Online Library, 2014, pp. 46-55.
[59] L. Lv, J. He, M. Wei, D.G. Evans, X. Duan, Factors influencing the removal of fluoride from aqueous solution by calcined Mg–Al–CO3 layered double hydroxides, Journal of Hazardous Materials, 133 (2006) 119-128.
[60] Z. Karami, S.M.R. Paran, P. Vijayan P, M.R. Ganjali, M. Jouyandeh, A. Esmaeili, S. Habibzadeh, F. J Stadler, M.R. Saeb, A Comparative Study on Cure Kinetics of Layered Double Hydroxide (LDH)/Epoxy Nanocomposites, Journal of Composites Science, 4 (2020) 111.
[61] Z. Karami, M.R. Ganjali, M. Zarghami Dehaghani, M. Aghazadeh, M. Jouyandeh, A. Esmaeili, S. Habibzadeh, A. Mohaddespour, K. Formela, J.T. Haponiuk, Kinetics of Cross-Linking Reaction of Epoxy Resin with Hydroxyapatite-Functionalized Layered Double Hydroxides, Polymers, 12 (2020) 1157.
[62] Z. Karami, M. Jouyandeh, S.M. Hamad, M.R. Ganjali, M. Aghazadeh, L. Torre, D. Puglia, M.R. Saeb, Curing epoxy with Mg-Al LDH nanoplatelets intercalated with carbonate ion, Prog. Org. Coat., 136 (2019) 105278.

[63] Z. Karami, M. Jouyandeh, J.A. Ali, M.R. Ganjali, M. Aghazadeh, M. Maadani, M. Rallini, F. Luzi, L. Torre, D. Puglia, M.R. Saeb, Development of Mg-Zn-Al-CO3 ternary LDH and its curability in epoxy/amine system, Prog. Org. Coat., 136 (2019) 105264.
[64] R. Ramasamy, Vibrational spectroscopic studies of imidazole, Armenian Journal of Physics, 8 (2015) 51-55.
[65] Y. Zhao, F. Li, R. Zhang, D.G. Evans, X. Duan, Preparation of layered double-hydroxide nanomaterials with a uniform crystallite size using a new method involving separate nucleation and aging steps, Chem. Mater., 14 (2002) 4286-4291.
[66] A. Oyarzabal, A. Mugica, A.J. Müller, M. Zubitur, Hydrolytic degradation of nanocomposites based on poly (l-lactic acid) and layered double hydroxides modified with a model drug, J. Appl. Polym. Sci., 133 (2016).
[67] E. Kanezaki, Intercalation of naphthalene-2, 6-disulfonate between layers of Mg and Al double hydroxide: Preparation, powder X-Ray diffraction, fourier transform infrared spectra and X-Ray photoelectron spectra, Materials research bulletin, 34 (1999) 1435-1440.
[68] P. Ding, B. Kang, J. Zhang, J. Yang, N. Song, S. Tang, L. Shi, Phosphorus-containing flame retardant modified layered double hydroxides and their applications on polylactide film with good transparency, Journal of colloid and interface science, 440 (2015) 46-52.
[69] F. Leroux, J.-P. Besse, Polymer interleaved layered double hydroxide: a new emerging class of nanocomposites, Chem. Mater., 13 (2001) 3507-3515.
[70] M. Jouyandeh, M.R. Ganjali, J.A. Ali, M. Aghazadeh, F.J. Stadler, M.R. Saeb, Curing epoxy with electrochemically synthesized MnxFe3-xO4 magnetic nanoparticles, Progress in Organic Coatings, 136 (2019) 105199.
[71] M. Jouyandeh, M.R. Ganjali, J.A. Ali, M. Aghazadeh, F.J. Stadler, M.R. Saeb, Curing epoxy with electrochemically synthesized NixFe3-xO4 magnetic nanoparticles, Prog. Org. Coat., (2019) 105198.
[72] M. Aliakbari, O.M. Jazani, M. Sohrabian, M. Jouyandeh, M.R. Saeb, Multi-nationality epoxy adhesives on trial for future nanocomposite developments, Progress in Organic Coatings, 133 (2019) 376-386.
[73] M.J. Shin, Y.J. Shin, J.S. Shin, Latent imidazole curing agents by microencapsulation with copolymers, Particulate Science and Technology, 36 (2018) 112-116.
[74] B.G. Soares, S. Livi, J. Duchet-Rumeau, J.-F. Gerard, Preparation of epoxy/MCDEA networks modified with ionic liquids, Polymer, 53 (2012) 60-66.
[75] R. Mitani, H. Yamamoto, M. Sumimoto, Theoretical study on the reaction mechanism of imidazole-catalyzed phenol-epoxy ring-opening reaction and the evaluation of catalyst performance, Chemical Physics Letters, 742 (2020) 137143.
[76] F. Tikhani, M. Jouyandeh, S.H. Jafari, S. Chabokrow, M. Ghahari, K. Gharanjig, F. Klein, N. Hampp, M.R. Ganjali, K. Formela, M.R. Saeb, Cure Index demonstrates curing of epoxy composites containing silica nanoparticles of variable morphology and porosity, Progress in Organic Coatings, 135 (2019) 176-184.
[77] V. Akbari, F. Najafi, H. Vahabi, M. Jouyandeh, M. Badawi, S. Morisset, M.R. Ganjali, M.R. Saeb, Surface chemistry of halloysite nanotubes controls the curability of low filled epoxy nanocomposites, Prog. Org. Coat., 135 (2019) 555-564.
[78] T. Ozawa, Applicability of Friedman plot, Journal of Thermal Analysis, 31 (1986) 547-551.
[79] H.E. Kissinger, Reaction kinetics in differential thermal analysis, Analytical chemistry, 29 (1957) 1702-1706.

[80] S. Vyazovkin, A.K. Burnham, J.M. Criado, L.A. Pérez-Maqueda, C. Popescu, N. Sbirrazzuoli, ICTAC Kinetics Committee recommendations for performing kinetic computations on thermal analysis data, Thermochim. Acta., 520 (2011) 1-19.
[81] J. Málek, The kinetic analysis of non-isothermal data, Thermochimica acta, 200 (1992) 257-269.
[82] S. Montserrat, J. Málek, A kinetic analysis of the curing reaction of an epoxy resin, Thermochimica acta, 228 (1993) 47-60.
[83] C.-F. Wang, Y.-C. Su, S.-W. Kuo, C.-F. Huang, Y.-C. Sheen, F.-C. Chang, Low-Surface-Free-Energy Materials Based on Polybenzoxazines, Angewandte Chemie International Edition, 45 (2006) 2248-2251.
[84] Y. Zhao, E.V. Barrera, Asymmmetric diamino functionalization of nanotubes assisted by BOC protection and their epoxy nanocomposites, Advanced Functional Materials, 20 (2010) 3039-3044.
[85] J. Yu, X. Huang, C. Wu, X. Wu, G. Wang, P. Jiang, Interfacial modification of boron nitride nanoplatelets for epoxy composites with improved thermal properties, Polymer, 53 (2012) 471-480.
[86] F. Hussain, J. Chen, M. Hojjati, Epoxy-silicate nanocomposites: cure monitoring and characterization, Materials Science and Engineering: A, 445 (2007) 467-476.
[87] G. Psarras, Conductivity and dielectric characterization of polymer nanocomposites, Physical Properties and Applications of Polymer Nanocomposites, Elsevier2010, pp. 31-69.
[88] E. Koufakis, G.N. Mathioudakis, A.C. Patsidis, G.C. Psarras, ZnTiO3/epoxy resin nanocomposites: Development, dielectric behaviour and functionality, Polymer Testing, 77 (2019) 105870.
[89] X. Zheng, D. Li, C. Feng, X. Chen, Thermal properties and non-isothermal curing kinetics of carbon nanotubes/ionic liquid/epoxy resin systems, Thermochimica acta, 618 (2015) 18-25.
[90] H. Bockhorn, A. Hornung, U. Hornung, Mechanisms and kinetics of thermal decomposition of plastics from isothermal and dynamic measurements, Journal of Analytical and Applied Pyrolysis, 50 (1999) 77-101.
[91] S.M.R. Paran, H. Vahabi, M. Jouyandeh, F. Ducos, K. Formela, M.R. Saeb, Thermal decomposition kinetics of dynamically vulcanized polyamide 6–acrylonitrile butadiene rubber–halloysite nanotube nanocomposites, Journal of Applied Polymer Science, 136 (2019) 47483.
[92] J.M. Criado, Kinetic analysis of DTG data from master curves, Thermochimica Acta, 24 (1978) 186-189.
[93] P. Das, P. Tiwari, Thermal degradation kinetics of plastics and model selection, Thermochimica Acta, 654 (2017) 191-202.

Fig. 1. (a) Synthesized IM and (b) modification of LDH by IM.

Fig. 2. (a) XRD pattern of the LDH and ionic liquid-modified LDH, **(b)** ATR of the LDH and LDH-IM and **(c)** TGA and DTG profiles of the LDH and ionic liquid-modified LDH.

Fig. 3. TEM images of dispersed LDH and LDH-IM into epoxy matrix.

Fig. 4. Nonisothermal DSC thermograms of epoxy nanocomposites containing 0.1 mass% of LDH and LDH-IM nanoparticles at different β of (a) 5, (b) 10 and (c) 15°C/min.

Fig. 5. Possible reaction between the imidazole and epoxy rings.

Fig. 6. Variation of E_α versus conversion for epoxy resin and prepared nanocomposites derived from (a) *Friedman* model and (b) *KAS* model.

Fig. 7. The storage modulus, loss modulus and tanδ alteration as a function of temperature at frequency of 1 Hz for EP, EP/LDH and EP/LDH-IM systems.

Fig. 8. (a) TGA and (b) DTG thermograms of neat epoxy and its nanocomposites.

Fig. 9. The evolution of activation energy against α based on *KAS* method.

Fig. 10. Theoretical master plots of different reaction models and experimental reduced rate plot at 5 ˚C/min for neat epoxy and its prepared nanocomposites.

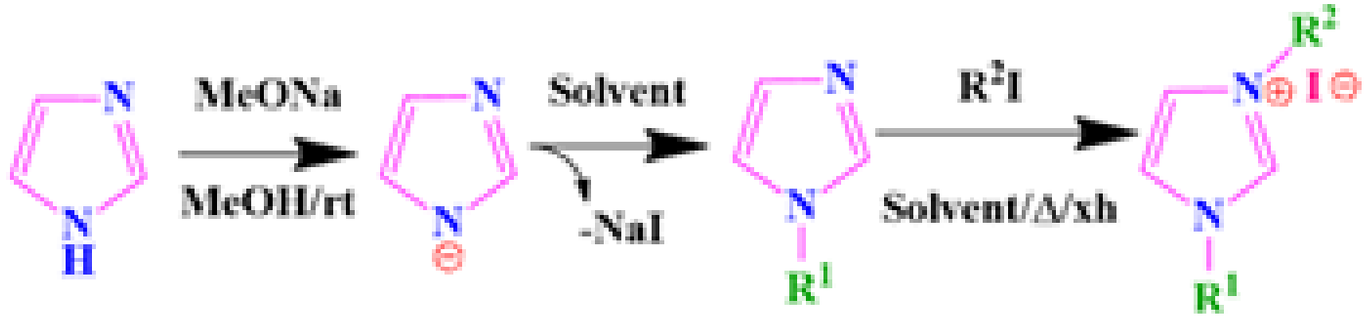
MeONa
MeOH/rt
Solvent
-NaI
R²I
Solvent/Δ/xh
R¹
R²

a)

IM:

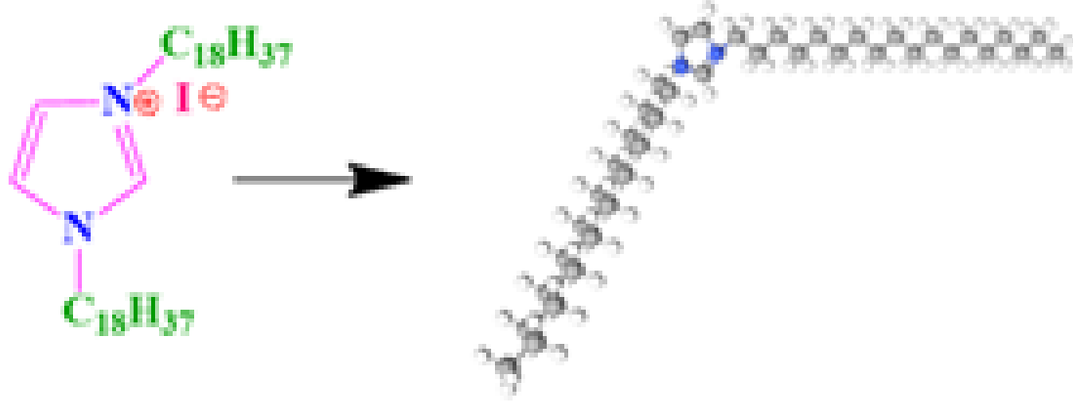
C18H37
C18H37

b)

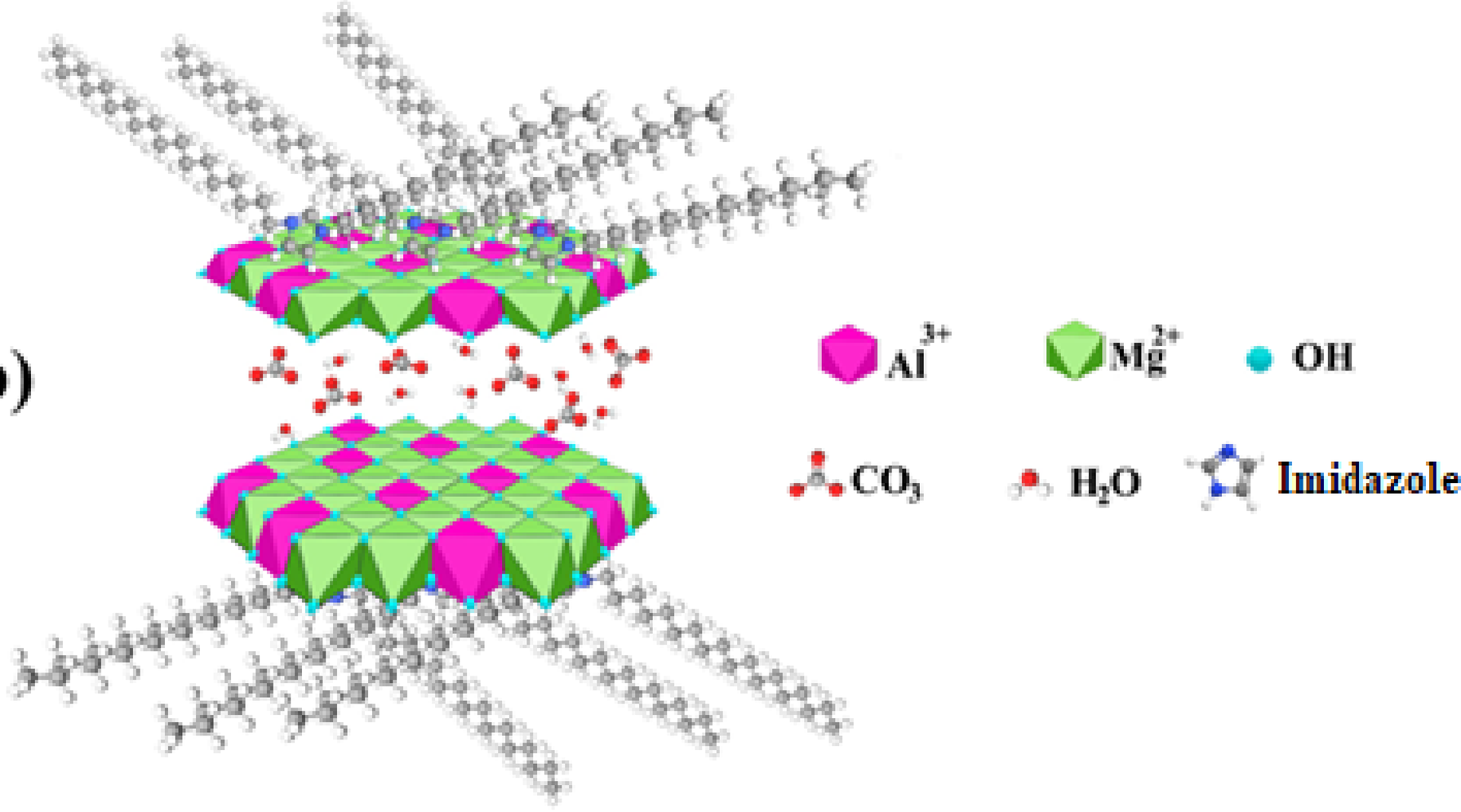
Al3+
Mg2+
OH
CO3
H2O
Imidazole

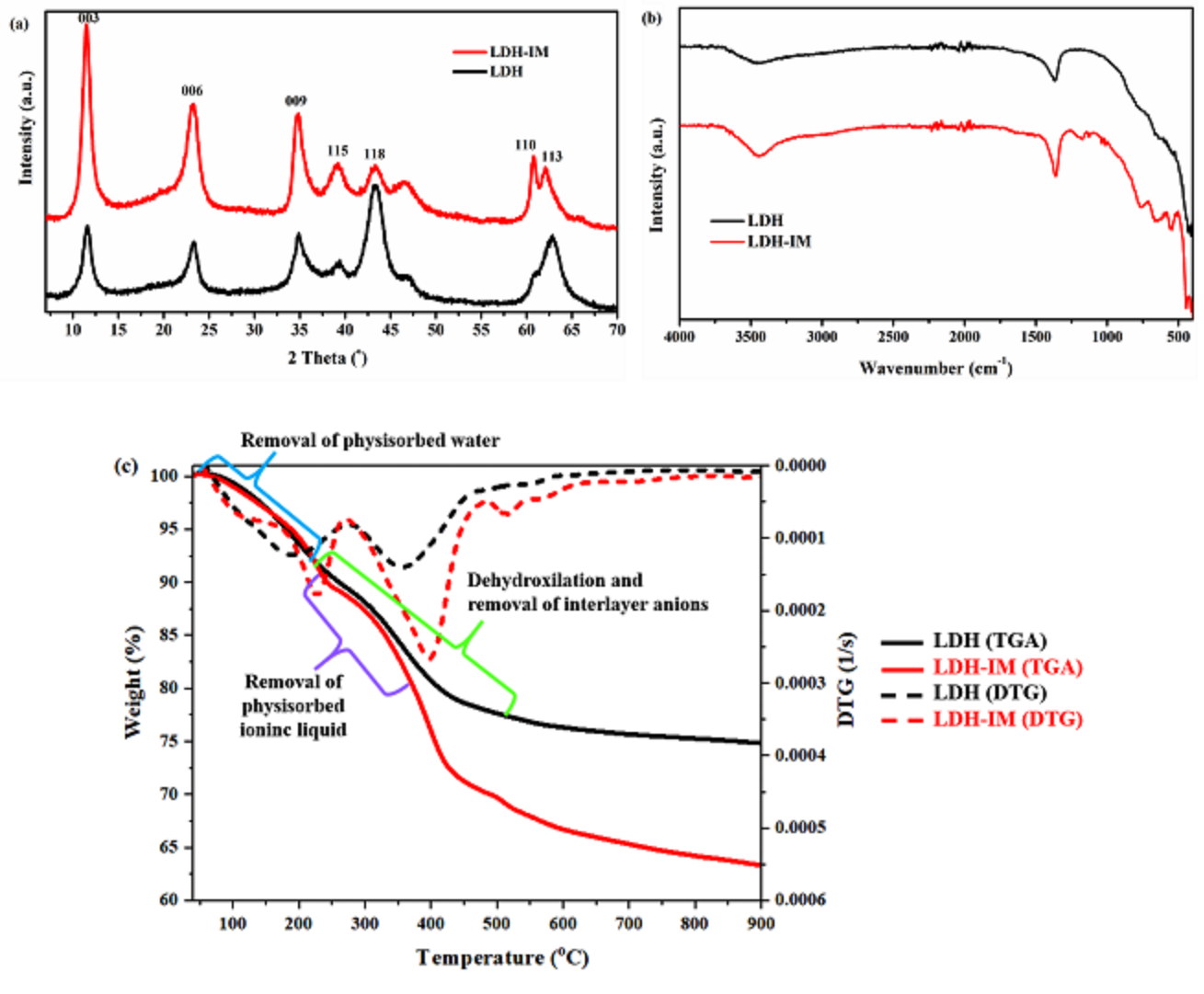
(a)
003
006
009
115
118
110
113
LDH-IM
LDH
Intensity (a.u.)
2 Theta (°)
(b)
LDH
LDH-IM
Intensity (a.u.)
Wavenumber (cm-1)
(c)
Removal of physisorbed water
Dehydroxilation and removal of interlayer anions
Removal of physisorbed ioninc liquid
Weight (%)
DTG (1/s)
Temperature (°C)
LDH (TGA)
LDH-IM (TGA)
LDH (DTG)
LDH-IM (DTG)

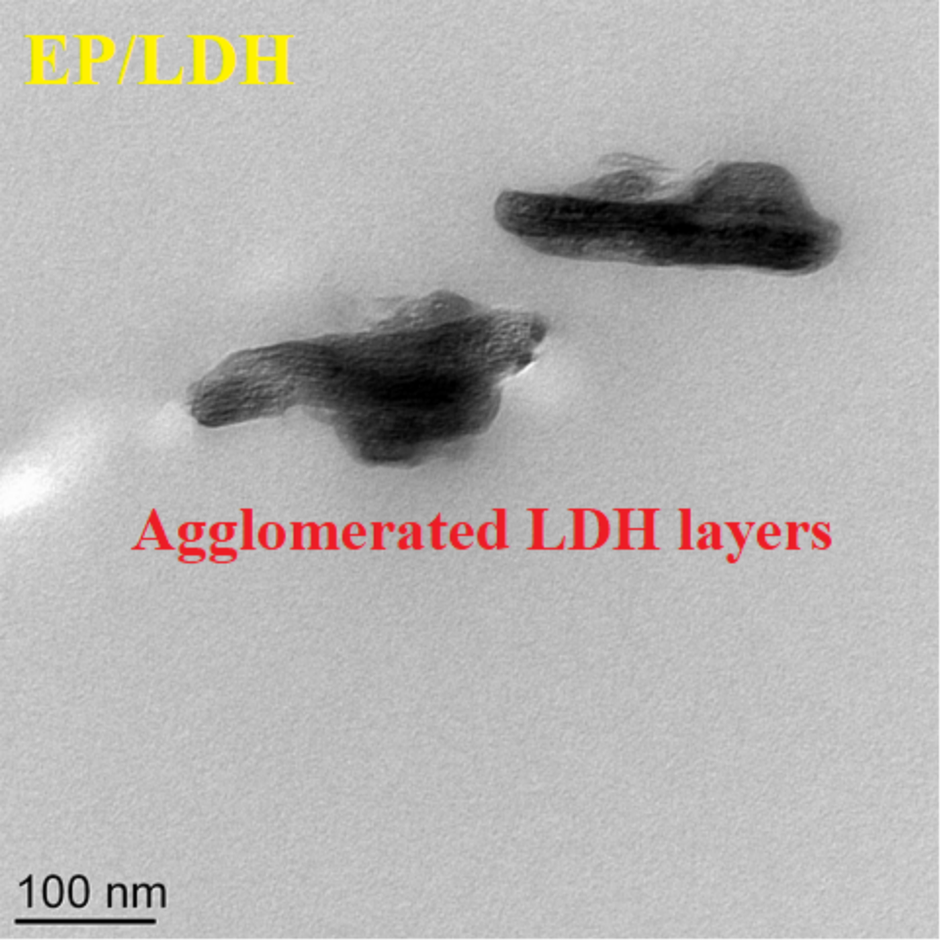
EP/LDH
Agglomerated LDH layers
100 nm

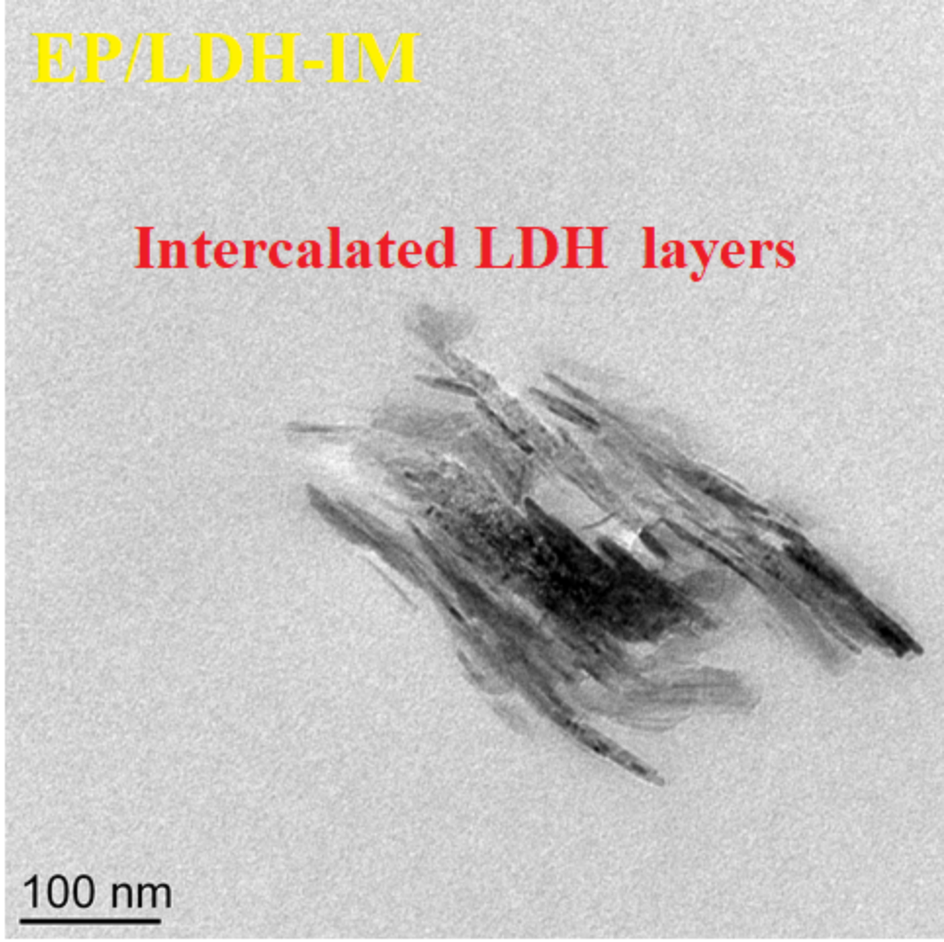
EP/LDH-IM
Intercalated LDH layers
100 nm

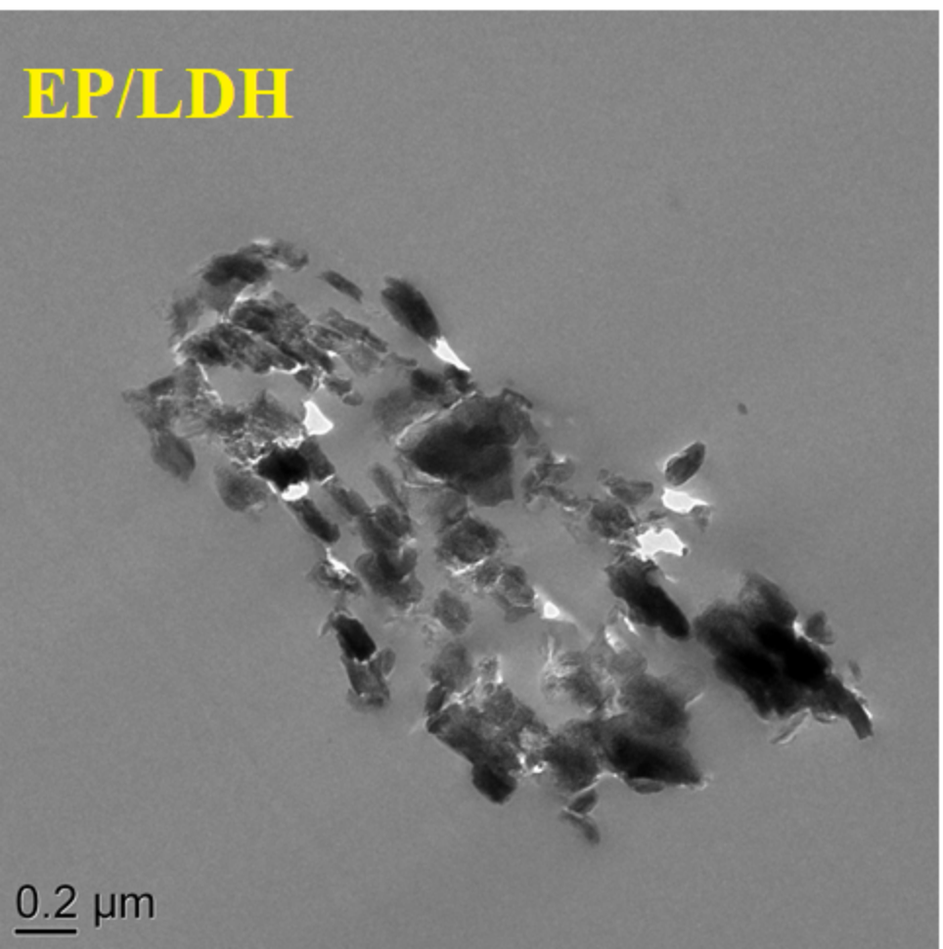
EP/LDH
0.2 μm

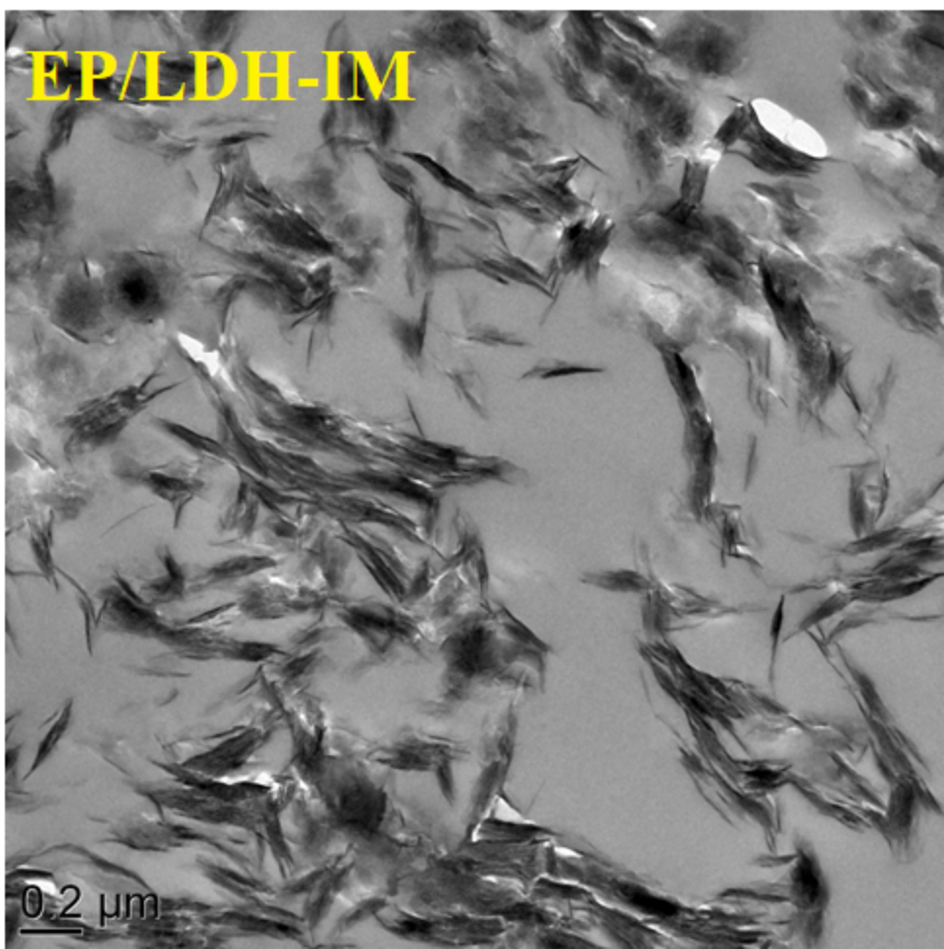
EP/LDH-IM
0.2 μm

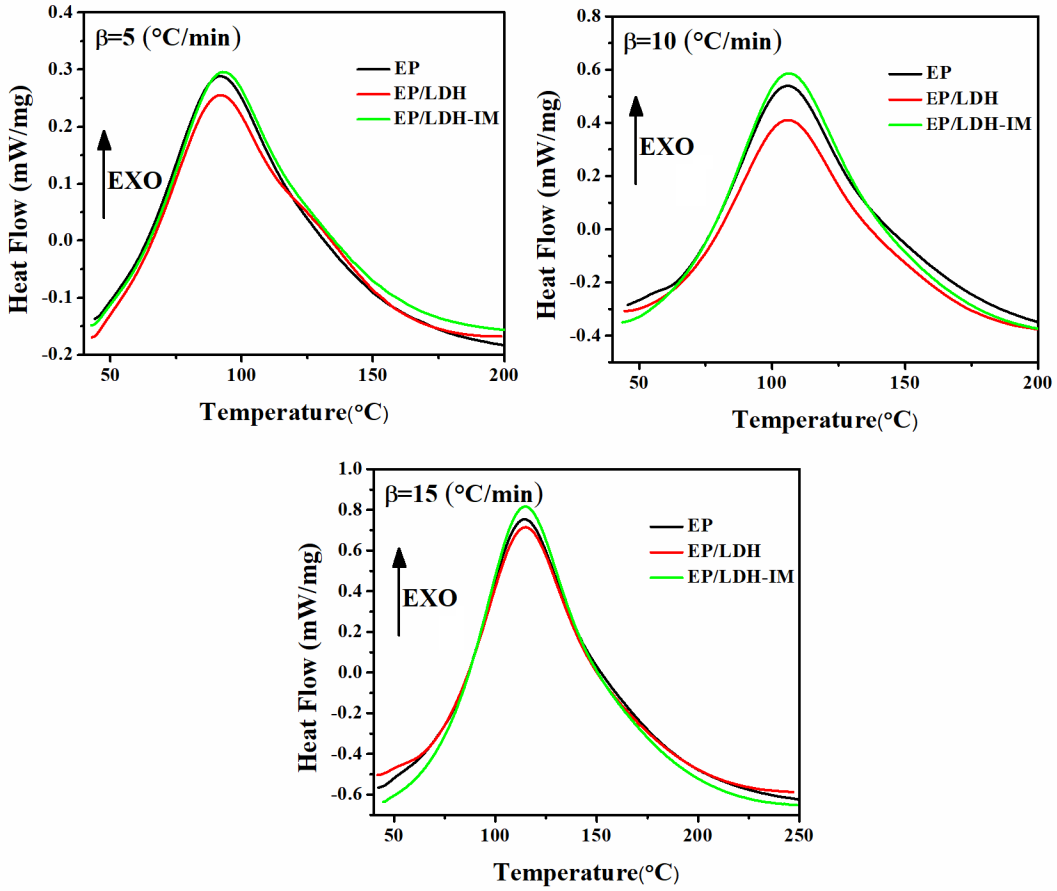
β=5 (°C/min)
EP
EP/LDH
EP/LDH-IM
EXO
Heat Flow (mW/mg)
Temperature(°C)
β=10 (°C/min)
EP
EP/LDH
EP/LDH-IM
EXO
Heat Flow (mW/mg)
Temperature(°C)
β=15 (°C/min)
EP
EP/LDH
EP/LDH-IM
EXO
Heat Flow (mW/mg)
Temperature(°C)

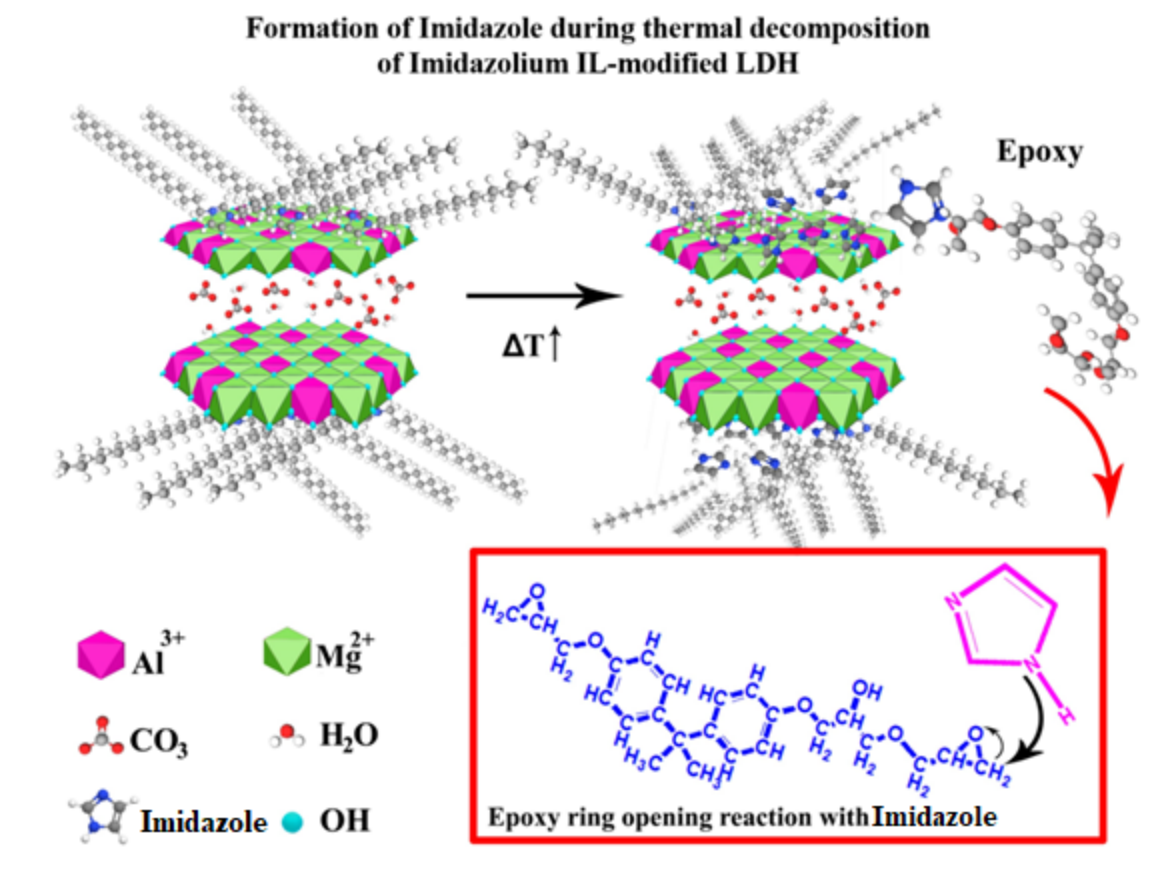
Formation of Imidazole during thermal decomposition
of Imidazolium IL-modified LDH
Epoxy
ΔT↑
Al3+
Mg2+
CO3
H2O
Imidazole
OH
Epoxy ring opening reaction with Imidazole

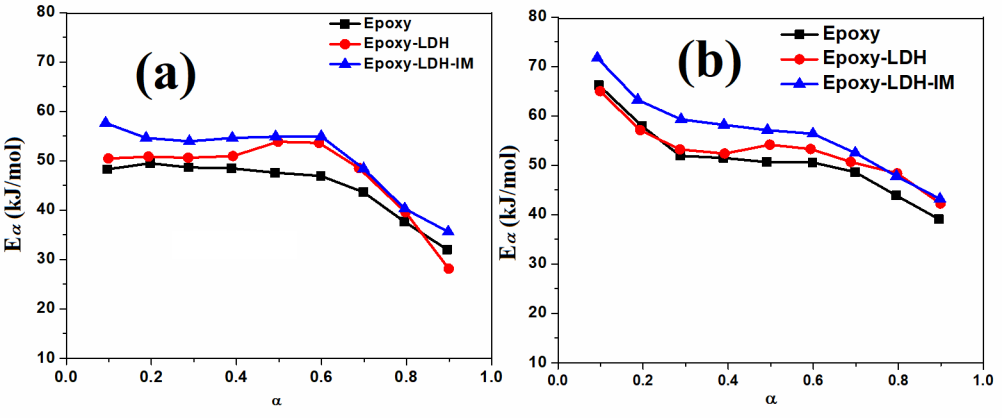
(a)
Epoxy
Epoxy-LDH
Epoxy-LDH-IM
Eα (kJ/mol)
α
(b)
Epoxy
Epoxy-LDH
Epoxy-LDH-IM
Eα (kJ/mol)
α

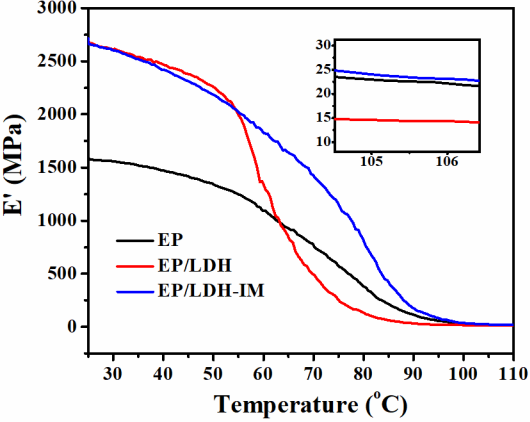
E' (MPa)
Temperature (°C)
EP
EP/LDH
EP/LDH-IM

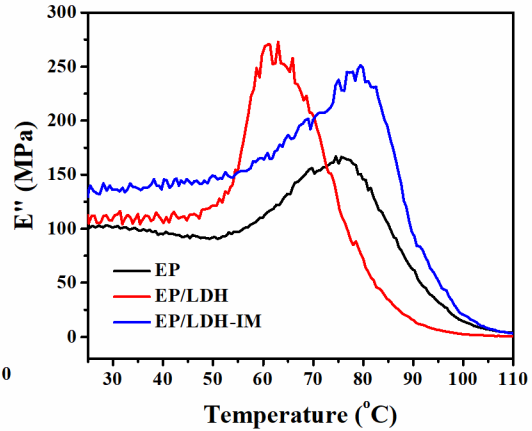
E'' (MPa)
Temperature (°C)
EP
EP/LDH
EP/LDH-IM

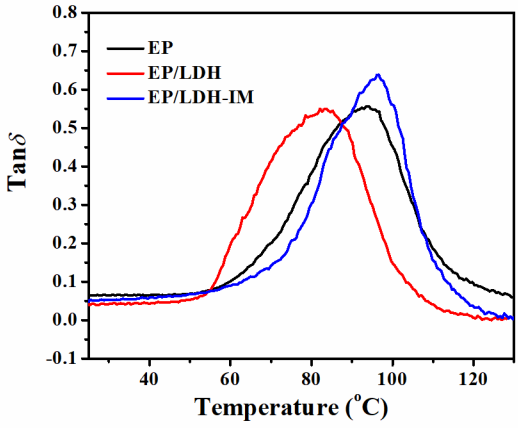
Tanδ
Temperature (°C)
EP
EP/LDH
EP/LDH-IM

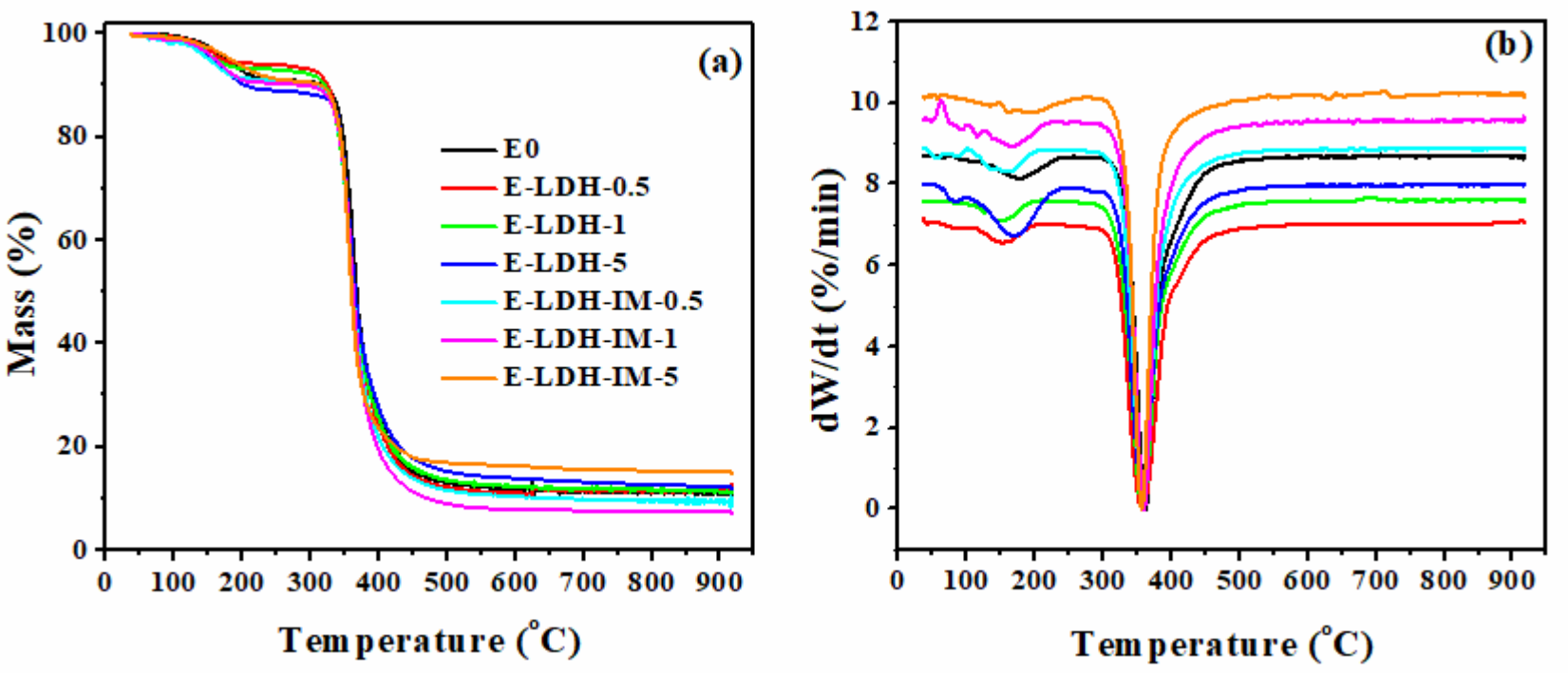
(a)
Mass (%)
Temperature (°C)
E0
E-LDH-0.5
E-LDH-1
E-LDH-5
E-LDH-IM-0.5
E-LDH-IM-1
E-LDH-IM-5
(b)
dW/dt (%/min)
Temperature (°C)

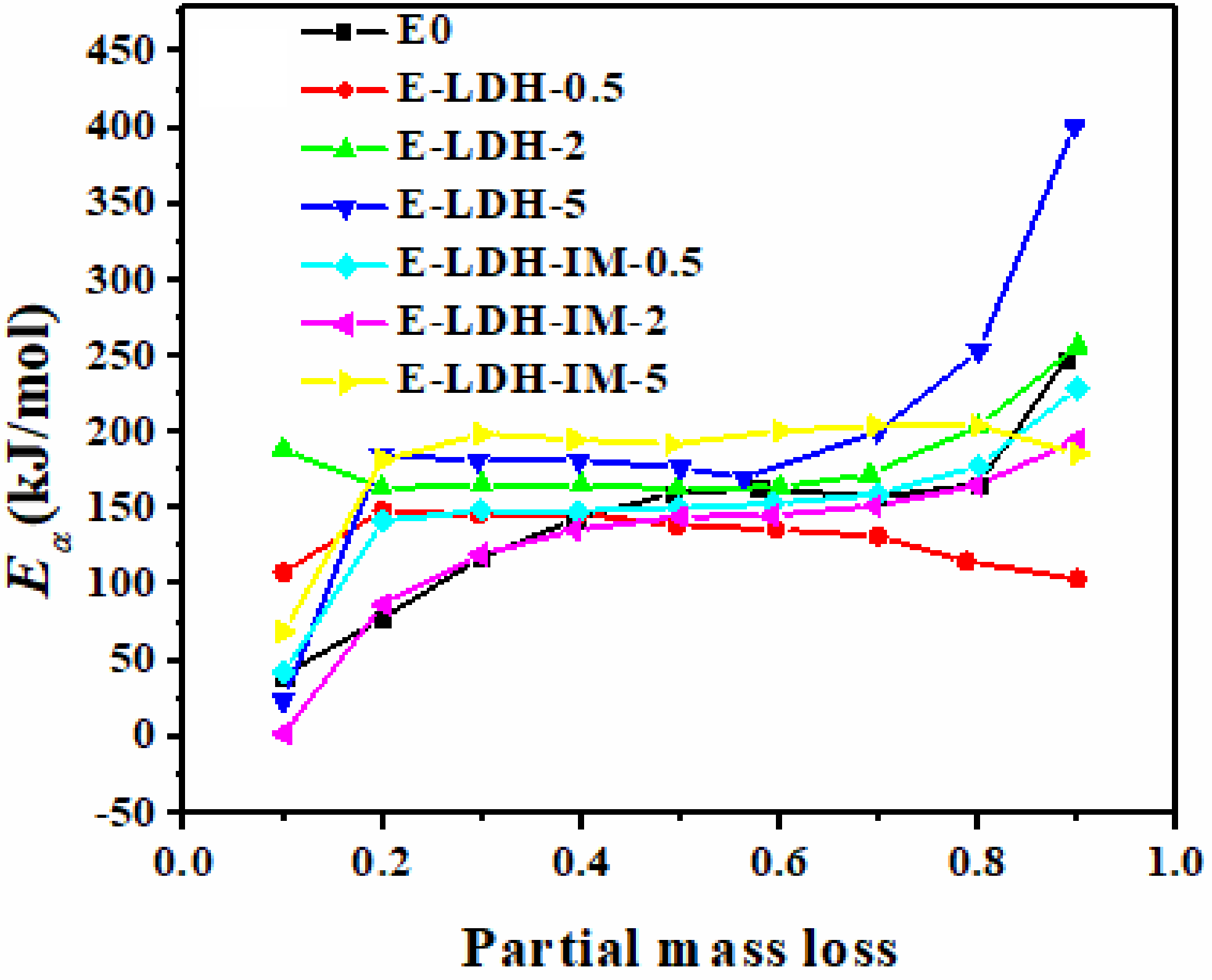
E0
E-LDH-0.5
E-LDH-2
E-LDH-5
E-LDH-IM-0.5
E-LDH-IM-2
E-LDH-IM-5
E_α (kJ/mol)
450
400
350
300
250
200
150
100
50
0
-50
0.0
0.2
0.4
0.6
0.8
1.0
Partial mass loss

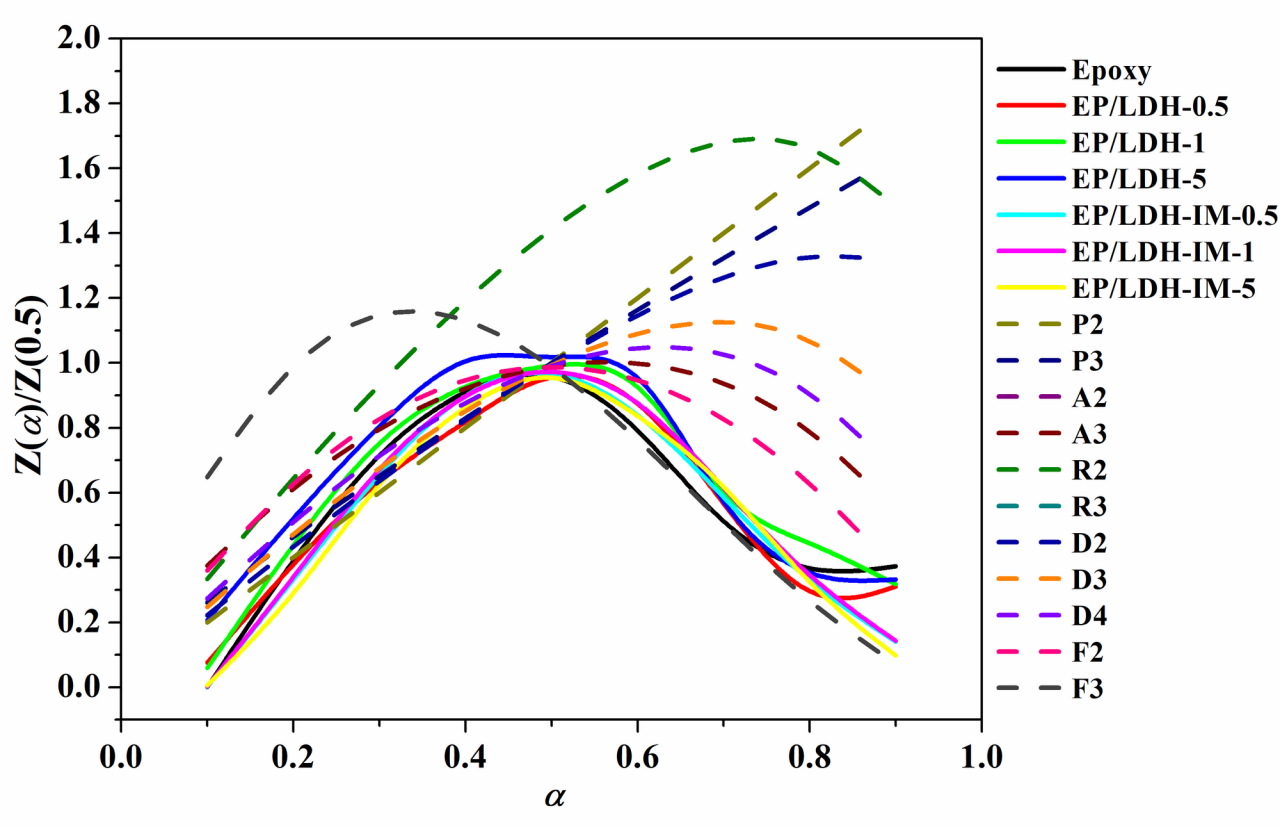
Z(α)/Z(0.5)
α
0.0
0.2
0.4
0.6
0.8
1.0
1.2
1.4
1.6
1.8
2.0
Epoxy
EP/LDH-0.5
EP/LDH-1
EP/LDH-5
EP/LDH-IM-0.5
EP/LDH-IM-1
EP/LDH-IM-5
P2
P3
A2
A3
R2
R3
D2
D3
D4
F2
F3

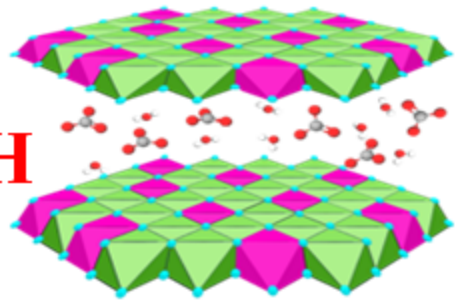

LDH

Hindered Curing Reaction of Epoxy
Decreased Glass Transition Temperature

Imidazolium Ionic
Liquids modified-LDH

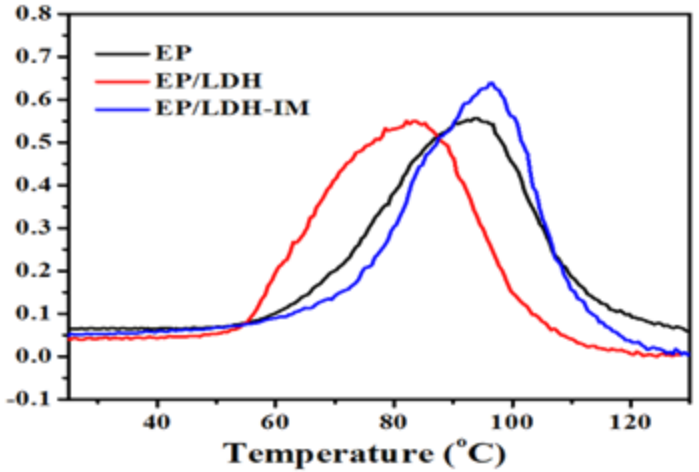

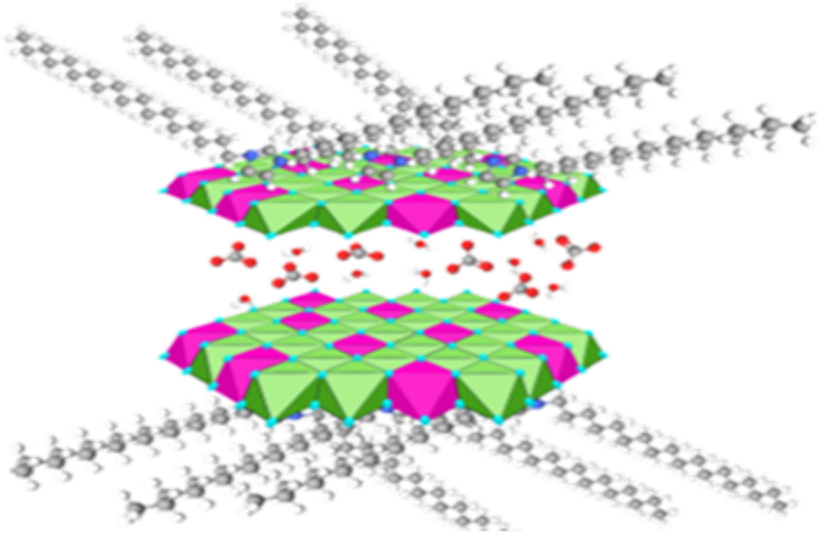

Facilitated Curing Reaction of Epoxy
Increased Glass Transition Temperature